UK Atomic Energy Authority

Applied Radiation Technology	Reference:	ART-24-16
	Issue:	1.4
	Date:	9th July 2024

GENERAL FUSION TBR ANALYSIS

ART-24-16

SUMMARY

This report details TBR analysis for General Fusion's MTF concept for fusion power. Simplified neutronics modelling, based on a small, dense magnetized Deuterium-Tritium plasma surrounded by a thick layer of liquid, breeder metal was performed. Lithium and lithium-lead were investigated as breeders, as well as different sizes of geometry. The activation and radiation damage of surrounding structures was also investigated.

	Name and Organisation	Signature	Date
Prepared By:	Hari Chohan Technology	Chohan, Hari [hchohan]	Digitally signed by Chohan, Hari [hchohan] Date: 2024.07.09 12:12:08 +01'00'
Approved By:	Tim Eade Technology	Eade, Tim [teade]	Digitally signed by Eade, Tim [teade] Date: 2024.07.09 13:51:28 +01'00'

Contents

1 Acronyms 3
2 Introduction 3
3 Method 3
3.1 Modelling 3
3.2 Outer Stainless Steel Structure 6
4 Results 8
4.1 Tritium Production 8
4.2 Nuclear Heating 13
4.3 Leakage Neutrons 14
4.4 Nuclide Inventory of the Liquid Metal 16
4.5 Surrounding Structure Radiation Damage 20
4.6 Surrounding Structure Activation 21
4.7 Trace Tritium and different Impurities 24
5 Conclusion 26
6 References 26
7 Appendix 28
7.1 Pulse Approximation 28
7.2 Tritium Production 29
7.3 Nuclear Heating 30
7.4 Leakage Neutrons 30
7.5 Surrounding Structure Radiation Damage 31
7.6 Surrounding Structure Activation 31
7.7 Nuclide inventory of the Liquid Metal (activities) (plots) 33
7.8 Nuclide Inventory of the Liquid Metal (masses) (plots) 35
7.9 Nuclide Inventory of the Liquid Metal (masses) (tables) 37

1 ACRONYMS

TBR: Tritium Breeding Ratio
MTF: Magnetized Target Fusion
D-T: Deuterium – Tritium
D-D: Deuterium – Deuterium
n: neutrons
s: seconds
MT: Reaction Type
DPA: Displacement Per Atom
SS: Stainless Steel
FDP: Fusion Demonstration Plant
LWR: Light Water Reactor
DEMO: DEMOnstration power plant

2 INTRODUCTION

In General Fusion's MTF concept for fusion power, a small, dense magnetized plasma of Deuterium-Tritium aims to reach fusion conditions when surrounded by a thick layer of liquid metal. Neutrons generated by fusion burn will be absorbed in the liquid metal liner, resulting in tritium breeding. This report details the effect of a Lithium or Lithium-Lead liquid metal liner on the expected Tritium Breeding Ratio. More information can be found in the statement of work [1].

3 METHOD

3.1 Modelling

Simple spherical geometry was used for this analysis consisting of a central void to represent the plasma source surrounded by a spherical shell of liquid metal. A final, external spherical 10cm layer of void completed the model. Three sizes of model were used, as described in Table 1 and a diagram of the geometry is shown in Figure 1.

Table 1: The sizes of the liquid metal shells for the different cases. The inner diameter also corresponds to the diameter of the source cavity.

Size	Inner Diameter [m]	Outer Diameter [m]
Small	0.4	4
Nominal	0.6	6
Large	0.8	8

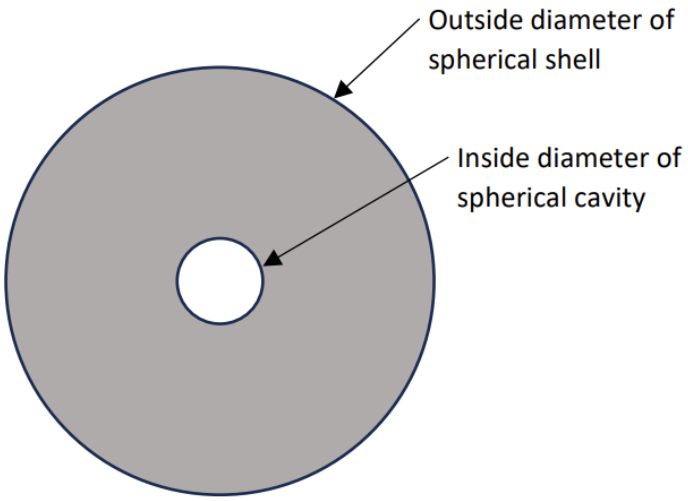

Figure 1: Spherical geometry modelled.

Two liquid metals were studied: natural lithium and a lithium-lead mix (84.2% Pb, 15.8% Li). The impurities in lithium, taken from the suppliers 1 and 2, are shown in Table 2. The Supplier 1 impurities were considered the main reference for the impurities, but Supplier 2 was also analysed for comparison. For all liquid metal material definitions, natural abundances of isotopes were used.

Table 2: The compositions of lithium provided by Supplier 1 and Supplier 2.

Element	Supplier 1 Weight %	Supplier 2 Weight %
Li	99.0	99.9
Na	0.9	0.02
K	0.05	0.005
Ca	0.04	0.02
Fe	0.01	0.005
Si	-	0.008
Al	-	0.005
Ni	-	0.003
Cu	-	0.004
Mg	-	0.01
N	-	0.02
Cl	-	0.006
Pb	-	0.003

The liquid metal processing is likely to be less than 100% efficient in extracting the tritium, leaving an estimated 40 ppb by mass tritium in the liquid metal [2]. This was included in one calculation to observe the effect of this trace.

For the radiation transport calculations, MCNP 6.2 was used with the FENDL 3.2b cross-section library. Calculations were performed separately for D-T and D-D reactions, in each simulation the neutron source was modelled as an isotropic, uniformly sampled sphere within the central cavity of 14.1 or 2.45 MeV neutron for the D-T and D-D reactions respectively. For this simplified modelling, the plasma material was not modelled, instead the source was modelled in vacuum inside the central cavity.

The operational scenario assumed for the MTF concept works uses pulses, each pulse lasts 1 s consisting of 700 µs irradiation with an average source strength of 3.23 E+23 n/s and 0.9993 s without irradiation. The liquid metal is cycled every 220 consecutive pulses. After these pulses the batch of liquid metal leaves the vessel and passes through a tritium extraction process, heat exchangers and undergoes some clean-up before entering the vessel again. The total amount of liquid metal is 10 times the amount in the vessel. Thus, each ‘batch’ of liquid metal is subjected to 10% of the neutron pulses over the lifetime of the machine. The lifetime of the machine was assumed to be 40 years. Thus, the average source strength for a batch of liquid metal over the lifetime of the machine is 2.261 E+19 n/s. In activation calculations, it is computationally expensive to model individual pulses over lifetimes of many pulses, > 1 E+08 in this case. Therefore, the pulses are averaged over the long lifetime which accurately calculates the activation of long-lived products. Then a short final period is included which accurately models the pulses to calculate the short-lived products. In these activation calculations of the liquid metal, the average source strength was used over the majority of the lifetime (40 years) except for the final 5 days where the pulses were modelled more accurately (220 s at 2.261 E+20 n/s followed by 1980 s off). The pulses were not modelled with full accuracy (3.23 E+23 n/s for 700 µs followed by 0.9993 s off) because computational limitations would only allow a few cycles (a few hours) to be modelled which wasn’t enough time to allow short-lived products to build up, whereas 5 days was long enough. An example comparison for these approaches is shown in appendix 7.1.

This source strength was assumed to be equal over all plasma sizes, therefore it was assumed to be more dilute in the large models and more concentrated in the small models. In fusion plasmas with ion temperatures of the order of 10 keV, the reactivity of D-D reactions is much lower than D-T reactions, as shown in Figure 2. For activation and DPA analysis, it was assumed that all of the source neutrons were D-T neutrons. The ion temperature of the plasma in General Fusion's machine may be different to this however, the D-T reaction is still likely to dominate over D-D.

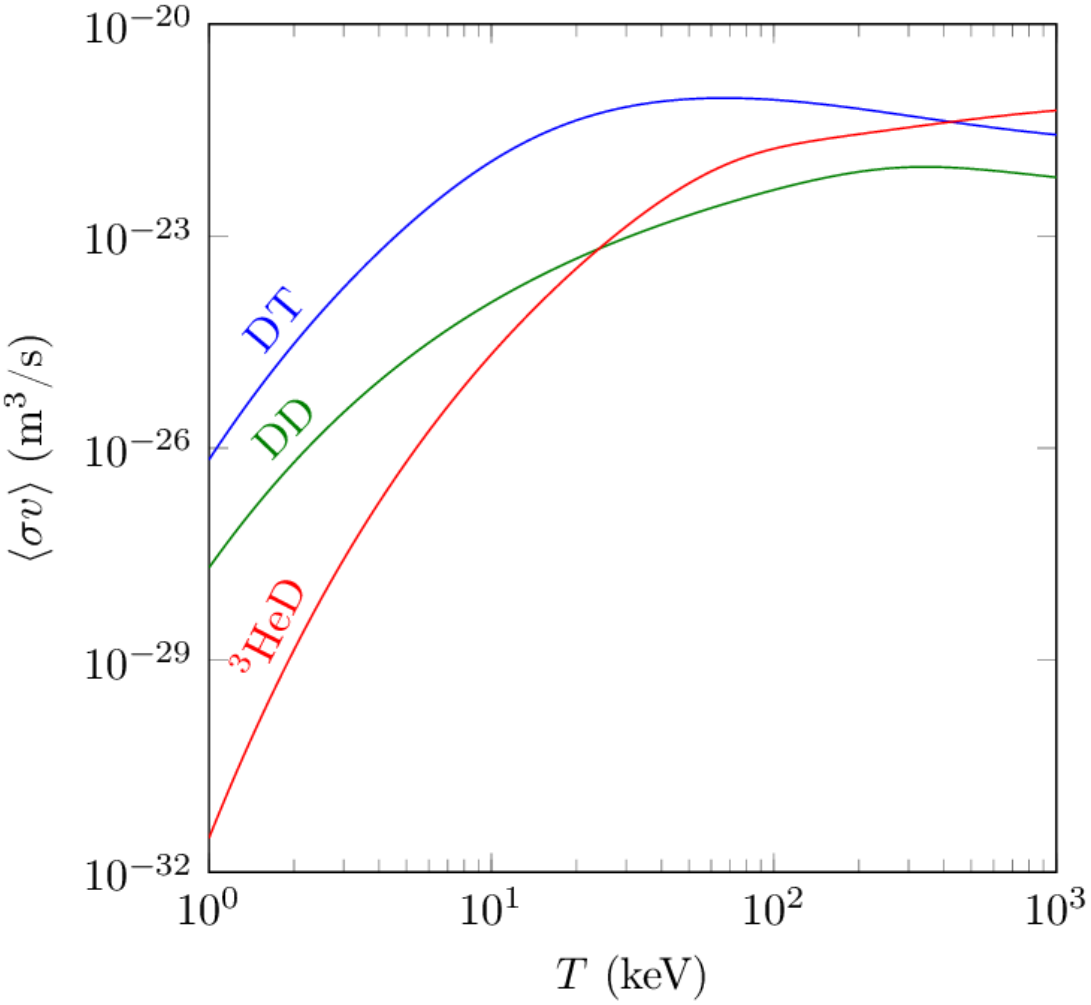

Figure 2: The reactivity of three fusion reactions involving hydrogen isotopes as a function of temperature [3].

The tritium production in the liquid metal was calculated using the MT number 205, corresponding to total tritium production. The liquid metal shell was modelled as concentric spheres of 10 cm thickness, the tritium production in each layer was calculated to determine the radial distribution of tritium production. Note that this is equivalent to modelling the liquid metal shell as one piece, it was only done to inspect the radial distribution of responses.

The thermal energy radial distribution (also known as nuclear heating) due to neutrons and photons was calculated using an energy deposition tally that tallied the energy deposition in each of the liquid metal layers.

The neutrons leaving the outer surface of the liquid metal were tallied using a surface current tally, grouped by the CCFE 709 energy group structure [4].

The neutron flux in the liquid metal was calculated using a cell flux tally, again grouped by the CCFE 709 energy group structure. The neutron flux was averaged over the concentric cells.

The neutron flux and the irradiation data were then used in FISPACT-II to calculate the nuclide inventory of the liquid metal after irradiation. The TENDL-2017 activation cross-section library was used.

3.2 Outer Stainless Steel Structure

To investigate the radiation effects on structures outside of the liquid metal, an external SS 316 shell was added to the models. The simulations described above were repeated with the addition of this shell, the dimensions listed in Table 3 and a diagram is shown in Figure 3.

Table 3: Dimensions of models with SS outer shells.

Size	Liquid Metal Inner Diameter [m]	Liquid Metal Outer Diameter / SS Shell Inner Diameter [m]	SS Shell Outer Diameter [m]
Small	0.4	4	5
Nominal	0.6	6	7
Large	0.8	8	9

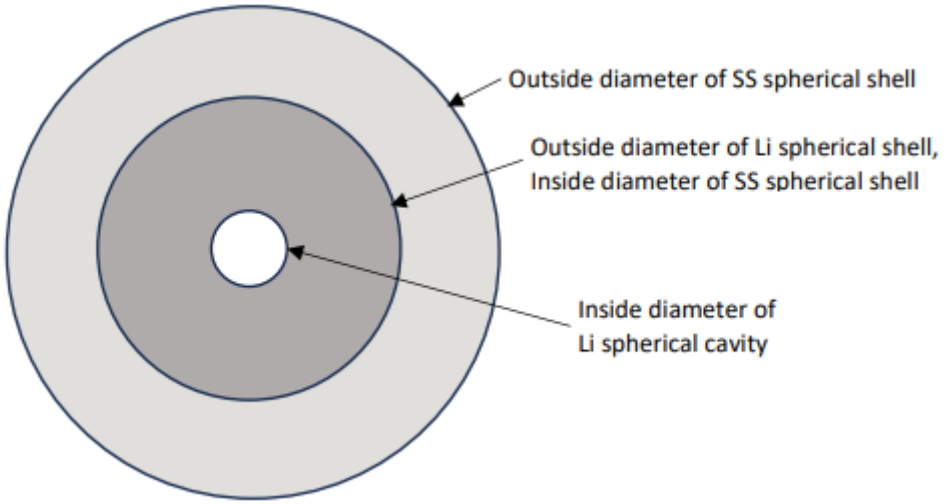

Figure 3: Spherical geometry with the surrounding SS 316 layer (not to scale).

The definition of SS 316 used was from AZO Materials [5]. This is a common grade of SS that doesn't have any specific considerations for low activation.

DPA tallies were added to the SS 316 shell using specific DPA cross-sections for SS 316 [6].

To investigate the radioactive waste produced in the SS 316 shell, the Canadian and UK waste classifications [7] [8] were used, shown in Table 4.

Table 4: Canadian and UK radioactive waste characterisation used in this analysis, interpreted from [7] and [8].

Waste Category	Canadian Definition	UK Definition
HLW	> 10^4 TBq / m^3 OR requires active cooling	Requires active cooling
ILW	> 400 Bq / g, < 10^4 TBq / m^3	> 12000 Bq/ g OR > 4000 Bq/ g (α)
LLW	< 400 Bq / g	< 12000 Bq/ g AND < 4000 Bq/ g (α)

In reality, the Canadian definition of LLW contains extra granularity, it is higher for certain beta/ gamma emitting radionuclides and rises to 4000 Bq / g for individual waste packages. However, this extra granularity was not used as the broad definition was assumed appropriate for this level of analysis. Furthermore, in this simple analysis, only the total activity definitions were used, i.e., not the alpha activity nor heating definitions.

The lifetime of the SS 316 structure was assumed to be 40 years, with 1 pulse per second.

In total, 26 different models were analysed, they are listed in Table 5.

Table 5: Parameters of the models studied.

Model	Reaction	Breeder Material	Trace Tritium [ppb]	Lithium Impurities (Supplier 1 or 2)	Breeder Outer Diameter [m]	SS Outer Diameter
Small Li DD	D-D	Lithium	0	1	4	-
Small Li DT	D-T	Lithium	0	1	4	-
Nominal Li DD	D-D	Lithium	0	1	6	-
Nominal Li DT	D-T	Lithium	0	1	6	-
Large Li DD	D-D	Lithium	0	1	8	-
Large Li DT	D-T	Lithium	0	1	8	-
Large Li DT H3	D-T	Lithium	40	1	8	-
Large Li DT Supplier 2	D-T	Lithium	0	2	8	-
Small PbLi DD	D-D	Lithium-Lead	0	1	4	-
Small PbLi DT	D-T	Lithium-Lead	0	1	4	-
Nominal PbLi DD	D-D	Lithium-Lead	0	1	6	-
Nominal PbLi DT	D-T	Lithium-Lead	0	1	6	-
Large PbLi DD	D-D	Lithium-Lead	0	1	8	-
Large PbLi DT	D-T	Lithium-Lead	0	1	8	-
Small Li DD SS	D-D	Lithium	0	1	4	5
Small Li DT SS	D-T	Lithium	0	1	4	5
Nominal Li DD SS	D-D	Lithium	0	1	6	7
Nominal Li DT SS	D-T	Lithium	0	1	6	7

Large Li DD SS	D-D	Lithium	0	1	8	9
Large Li DT SS	D-T	Lithium	0	1	8	9
Small PbLi DD SS	D-D	Lithium-Lead	0	1	4	5
Small PbLi DT SS	D-T	Lithium-Lead	0	1	4	5
Nominal PbLi DD SS	D-D	Lithium-Lead	0	1	6	7
Nominal PbLi DT SS	D-T	Lithium-Lead	0	1	6	7
Large PbLi DD SS	D-D	Lithium-Lead	0	1	8	9
Large PbLi DT SS	D-T	Lithium-Lead	0	1	8	9

4 RESULTS

Calculations were performed separately for D-T and D-D. The results are quoted per source neutron except results which look at activation and radiation damage, where the source rate is factored in to give lifetime results.

The data used for these results is provided in the accompanying spreadsheet and data files.

4.1 Tritium Production

The overall tritium production for the different models is shown in Figure 4 for D-D neutrons and Figure 5 for D-T neutrons, the numerical values are included in the appendix 7.2.

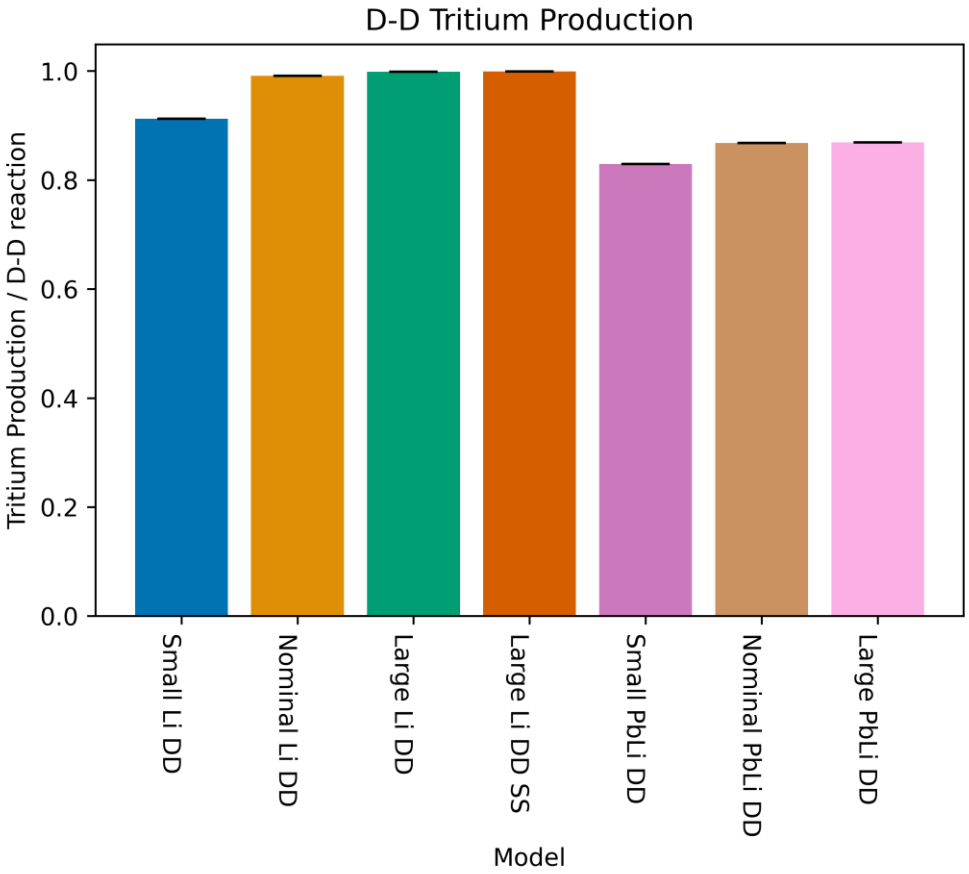

Figure 4: The tritium production per D-D neutron for the different models.

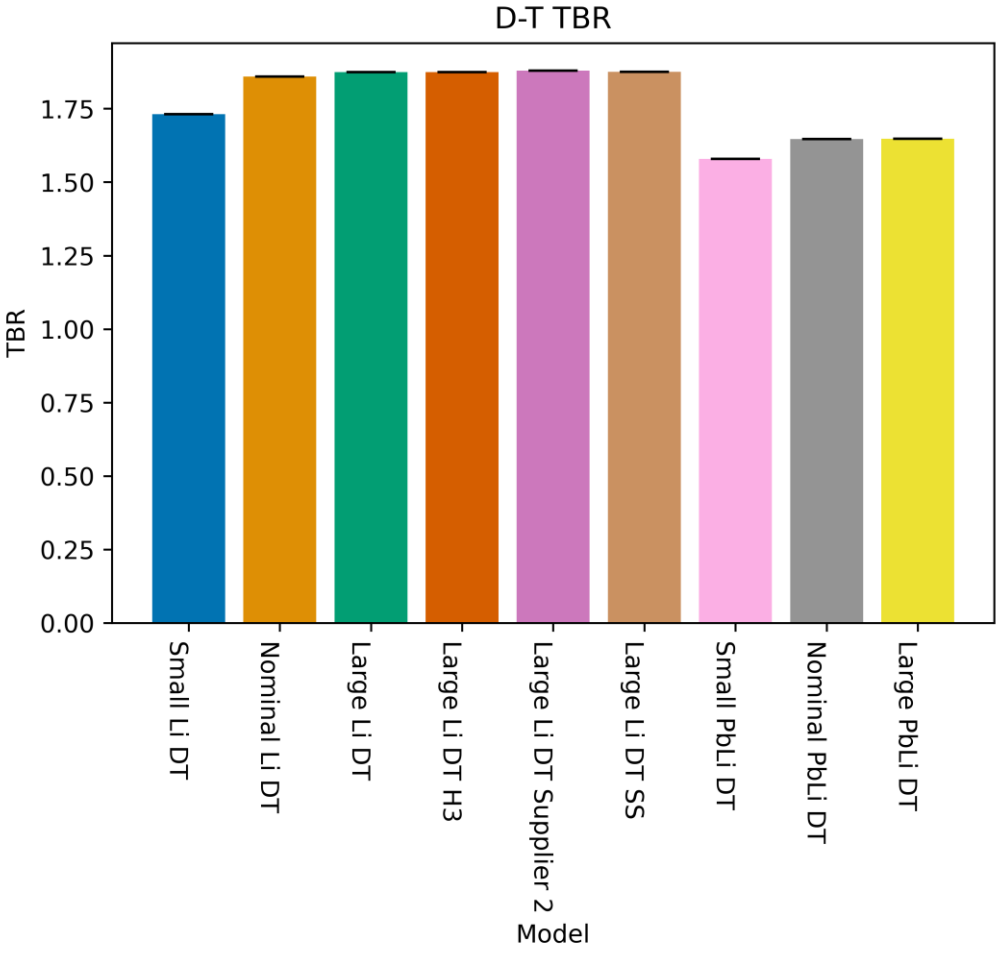

Figure 5: The TBRs for the different models for D-T neutrons.

These results are per source neutron (i.e., fusion reaction), hence, for D-T it refers to TBR but for D-D it refers to tritium production per D-D reaction. The D-T tritium production rate is higher than the D-D rate, furthermore as noted earlier, the D-D reaction is significantly less likely than the D-T reaction (for tokamaks with ion temperatures in the 10s keV it is approximately 10 times less likely), so D-T tritium production is much higher than in D-D.

To get a TBR value which accounts for neutrons from the D-D reaction (TBR_{DT+DD}) it is necessary to multiply the D-D Tritium production value (TPR_{DD}) by the ratio of D-D neutrons (n_{DD}) to D-T neutrons (n_{DT}) and then add it to the D-T TBR value (TBR_{DT}). The formula for doing this is given below in Equation 1.

$$TBR_{DT+DD} = TBR_{DT} + TPR_{DD} \times \frac{n_{DD}}{n_{DT}}$$

Equation 1

The D-T TBR values are all above 1.5. Assuming a 100% efficient tritium retention cycle, a TBR value of ≥ 1.0 ensures tritium self-sufficiency. A TBR value of 1.1 is considered a good target to ensure tritium self-sufficiency considering inefficiencies in the tritium cycle in a full engineering model [9]. Since these analyses were conducted on simplified, representative geometries, the TBR values are optimistic and may reduce when more realistic engineering geometries are modelled.

The results show that the larger the dimension of the spherical breeder shell, the higher the tritium production rate, although there are diminishing returns as fewer neutrons make it to the back to breed tritium. The results also show that pure lithium gives a higher tritium production rate than lithium-lead. This is in part due to the ^{7}Li(n,n't)^{4}He reaction which has a threshold neutron energy at about 3 MeV (see Figure 8). With no first wall or structural materials to slow the neutrons down, and natural lithium, which is mostly (~92 at%) ^{7}Li, a significant number of the reactions produce a not only a triton but also an additional neutron. These additional neutrons can then produce more tritium from the ^{6}Li(n,t)^{4}He non-threshold reaction.

Having excess tritium, different impurities or the surrounding SS structure has minimal effect on the overall tritium production rate.

The radial distributions of tritium production are shown in Figure 6 for D-D and Figure 7 for D-T.

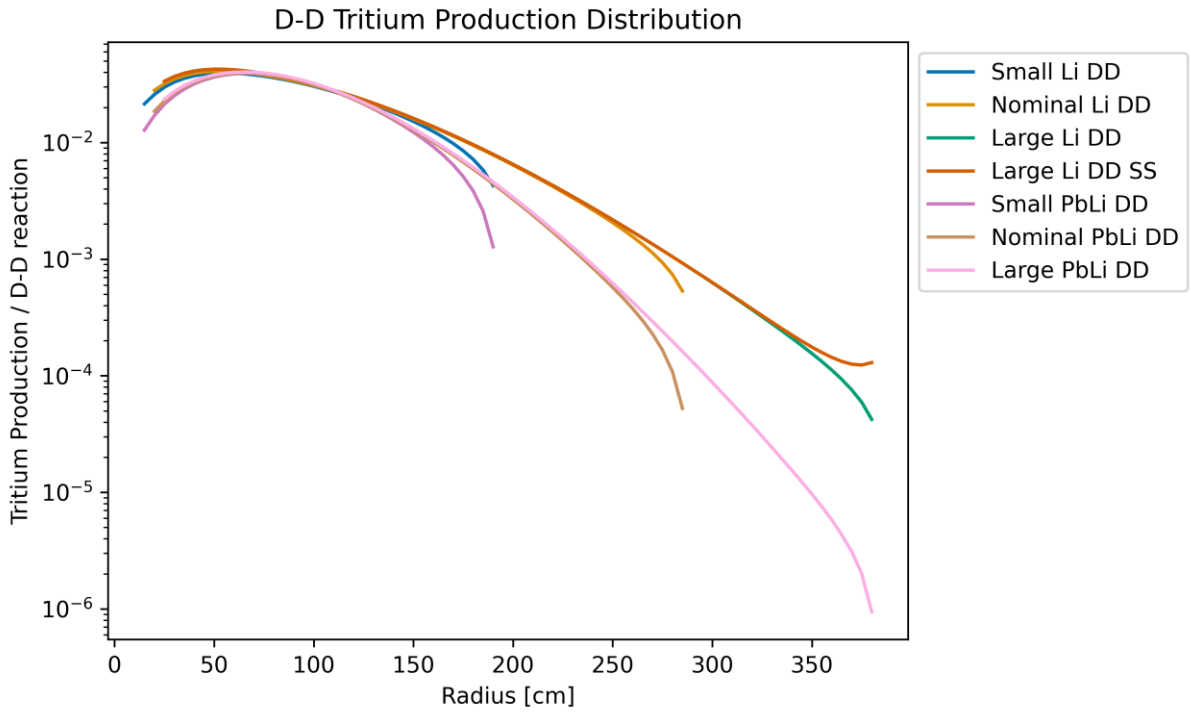

Figure 6: The radial distribution of tritium production for the different models for D-D neutrons.

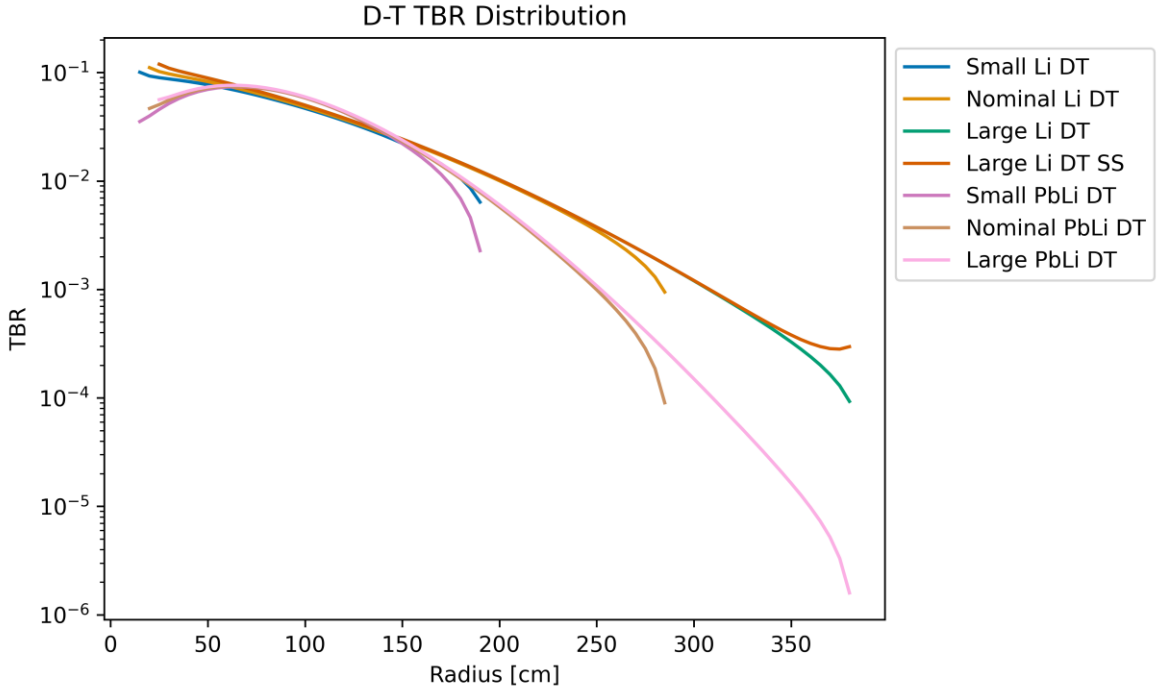

Figure 7: The radial distribution of TBRs for the different models for D-T neutrons.

The radial distributions of tritium production are similar shapes for both fusion reactions, with the production generally dropping off as a function of distance. All D-D models show a slight peak at about 50 cm, whereas for the D-T models a similar peak is only seen in the lithium-lead models. The peak is explained by the tritium production cross-sections shown in Figure 8. The cross-section for lithium-7 has a threshold at about 3 MeV which is above the D-D neutron energy therefore tritium is only produced from Li-6 in D-D. The Li-6 cross-section shows that neutron moderation increases the tritium production, and this is why the small peaks are seen in Figure 6. Similarly, the lithium-lead moderates the 14.1 MeV D-T quite effectively (this is also shown in Figure 13), meaning that the Li-7 reaction pathway is greatly reduced so, again, Li-6 dominates which benefits from neutron moderation. However, lithium

does not moderate the 14.1 MeV neutrons much and so the Li-7 path is more available. So, the tritium production is immediately high in the breeder so there is not the delayed small peak.

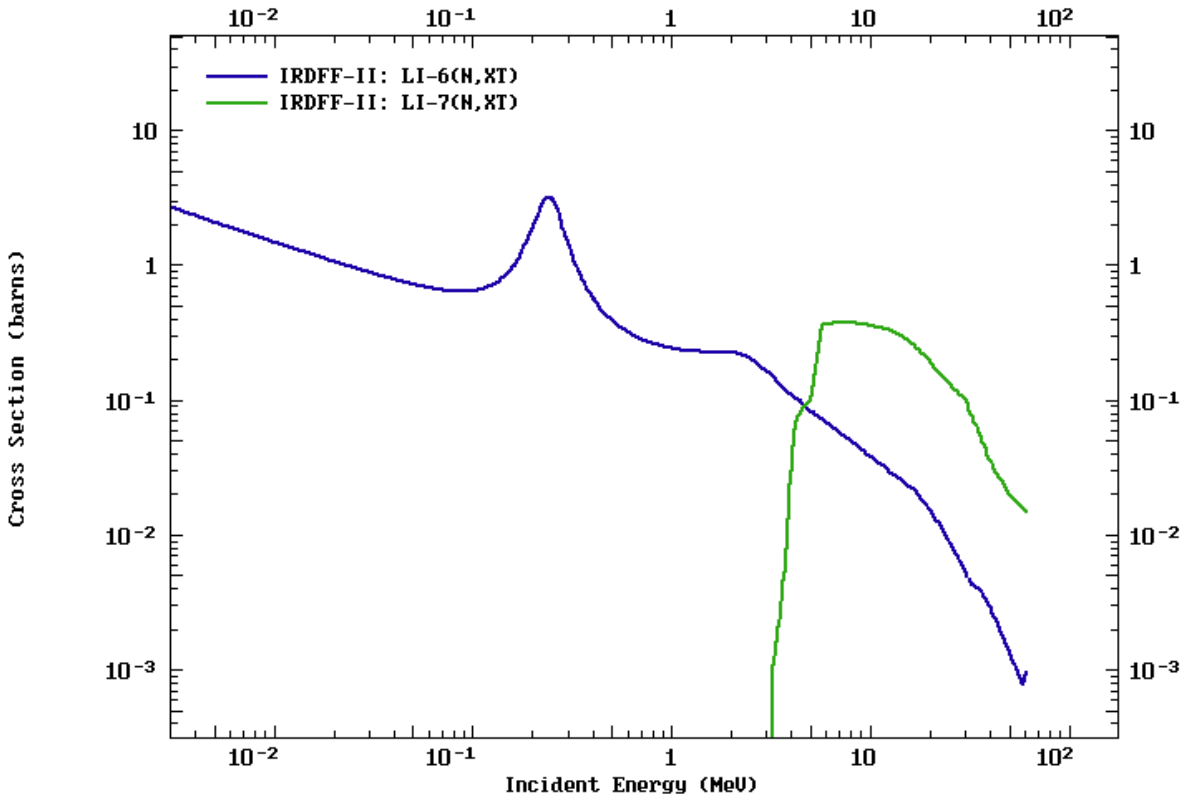

Figure 8: The tritium production cross-sections for lithium.

The effects of having trace tritium or different impurities in the lithium on the tritium production distribution are discussed in detail in section 4.7 but both had a minimal effect. Adding the surrounding SS structure has the small effect of increasing the tritium production at the boundary due to reflection of neutrons.

4.2 Nuclear Heating

The nuclear heating radial distributions are shown in Figure 9 and Figure 10, the total heating values are included in the appendix 7.3.

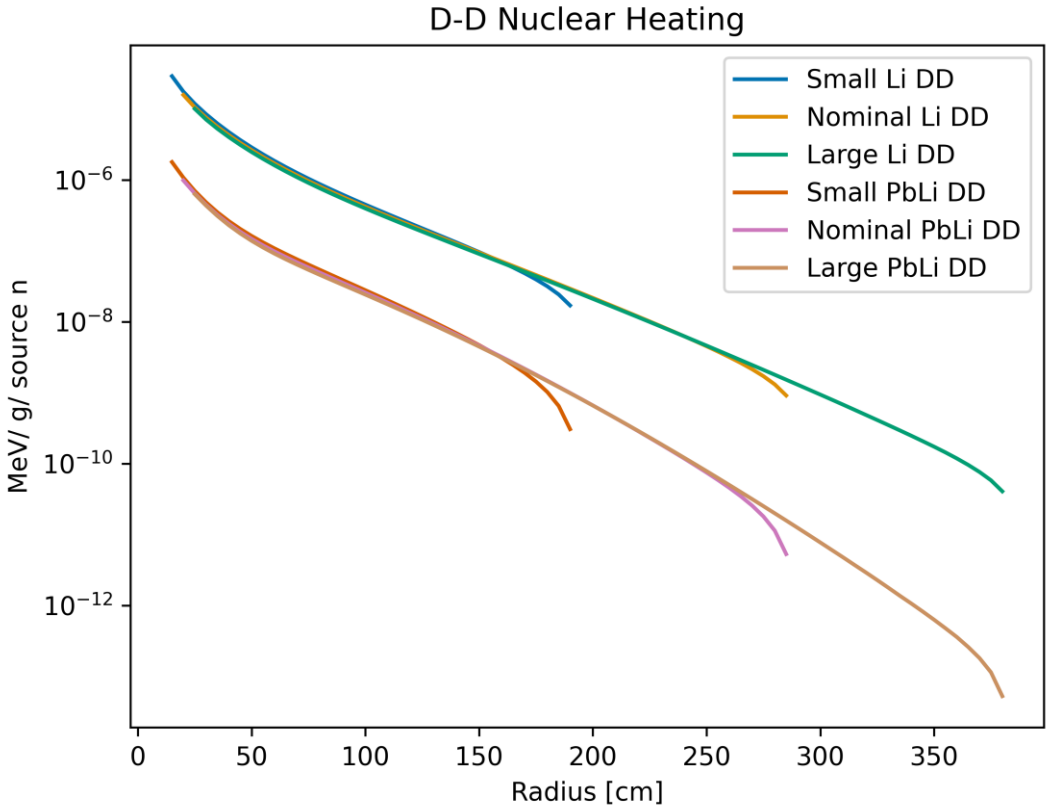

Figure 9: The radial distribution of D-D nuclear heating in the models.

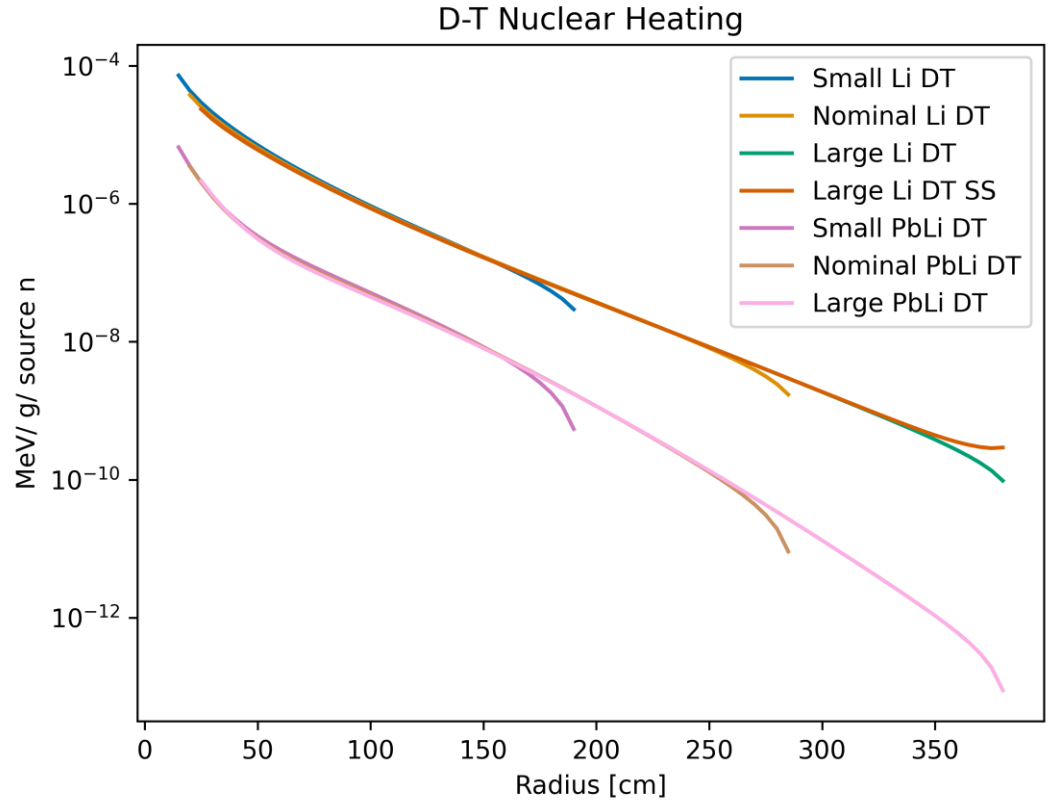

Figure 10: The radial distribution of D-T nuclear heating in the models.

The radial distributions of nuclear heating in the models generally follow the same shape, dropping off with distance as the neutrons are attenuated. The heating in the lithium-lead models is lower than in the lithium models and the heating due to D-D is slightly lower than due to D-T. The surrounding SS structure has the small effect of increasing the nuclear heating at the boundary due to reflection of radiation.

These results are per source neutron. Therefore, dividing by the source neutron energy (14.1 or 2.45 MeV) will give the energy multiplication results per gram.

Having trace tritium or different impurities in the lithium had minimal effects on the nuclear heating, this is discussed in section 4.7.

4.3 Leakage Neutrons

The fractions of neutrons leaving the liquid metal for the models are shown in and their spectra are shown in Figure 11, Figure 12 and Figure 13. The values are included in the appendix 7.4

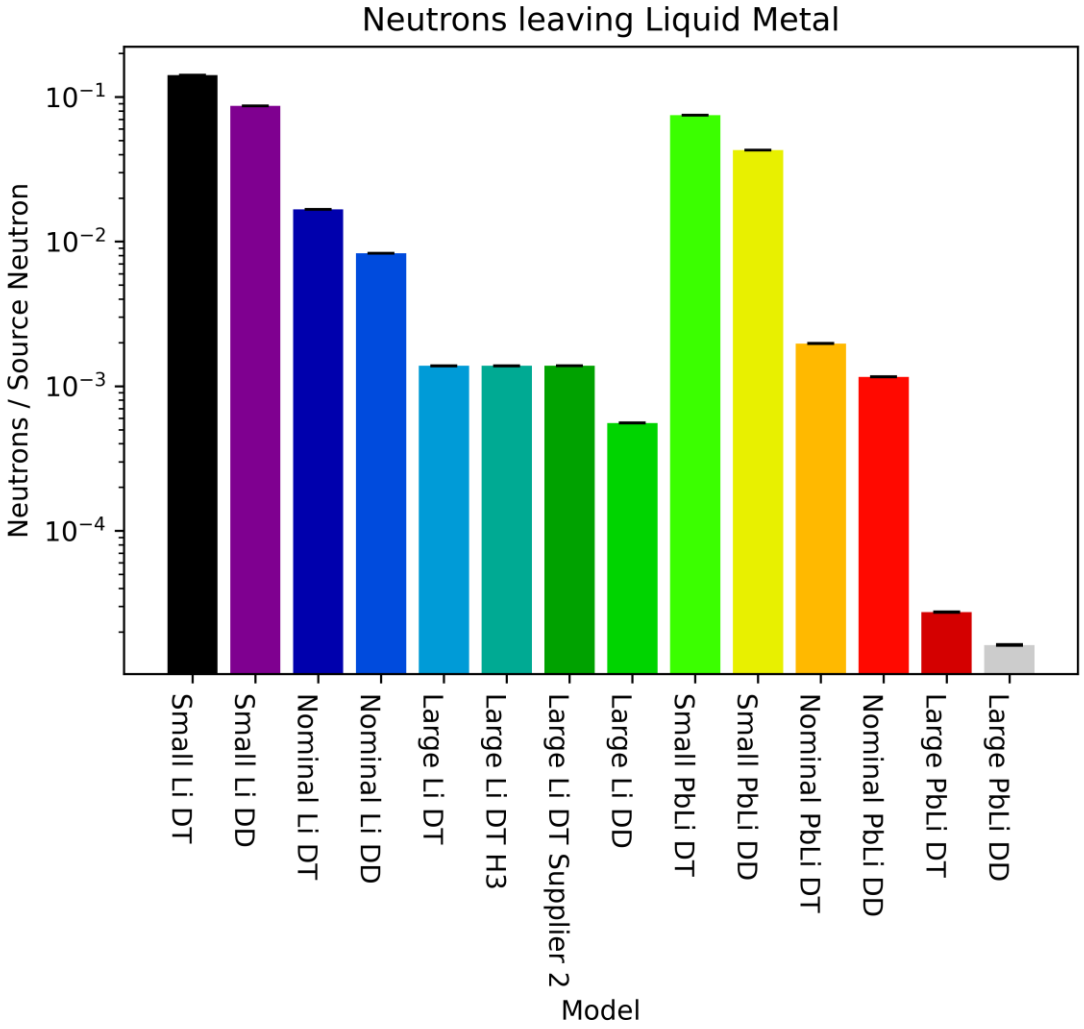

Figure 11: The fraction of neutrons leaving the liquid metal in the models.

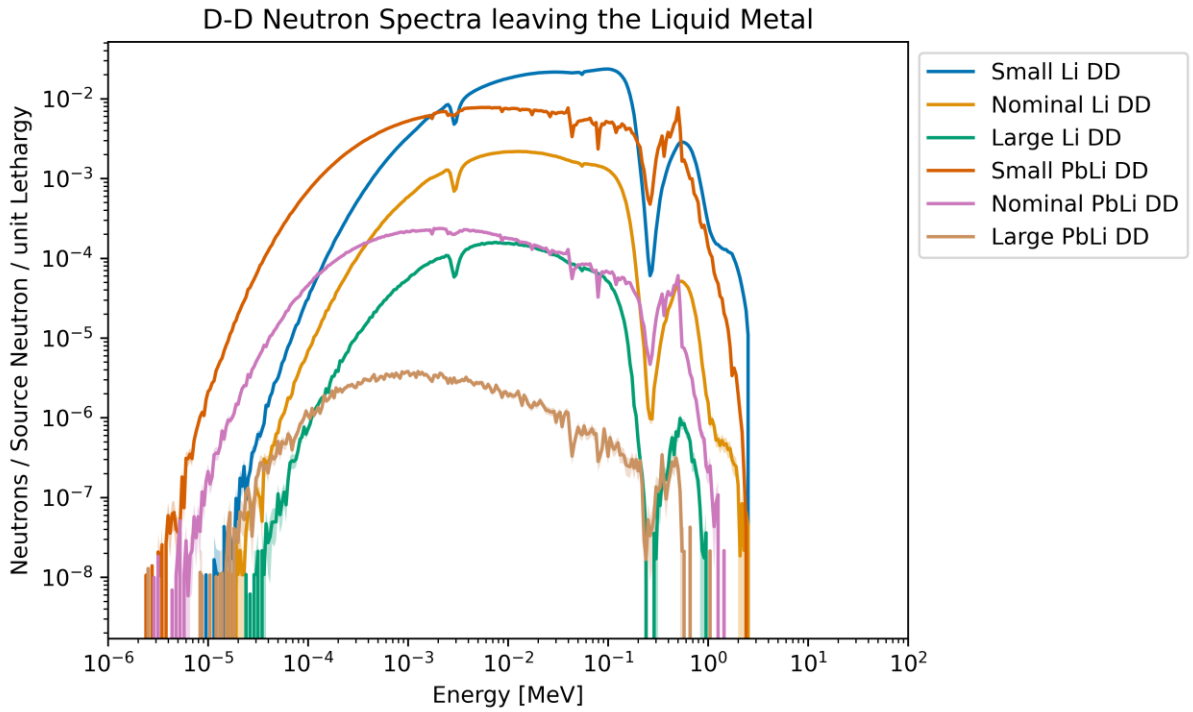

Figure 12: The spectra of D-D neutrons leaving the liquid metal for the models.

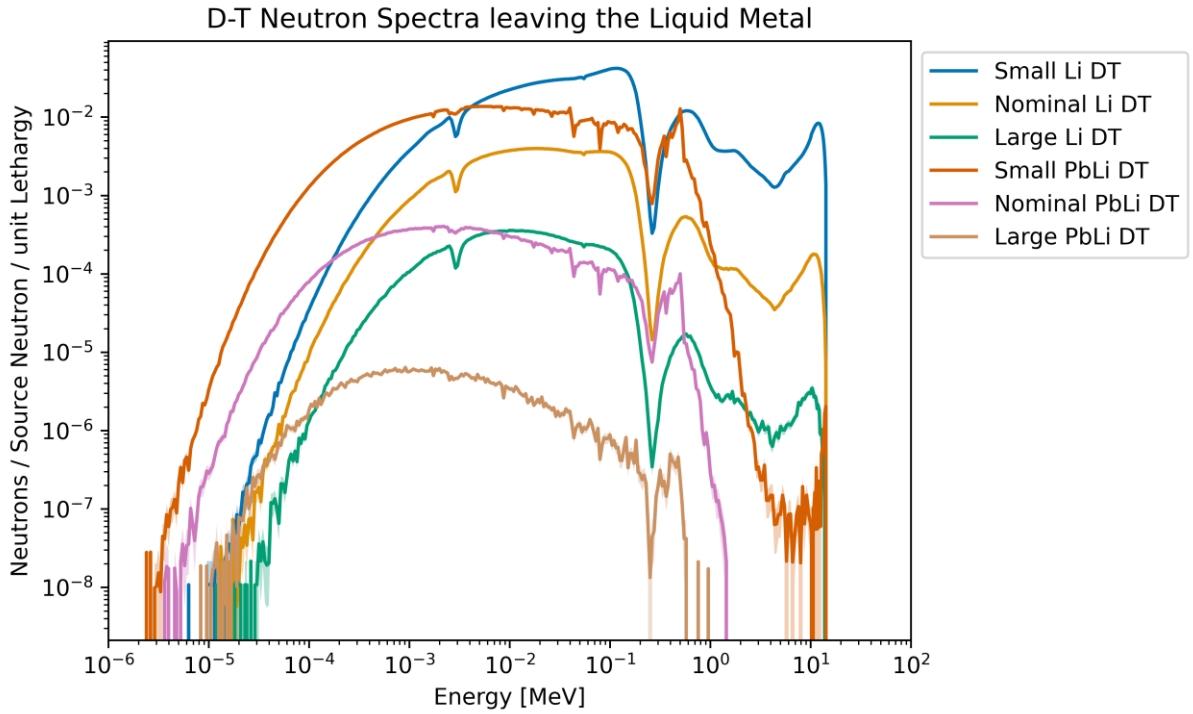

Figure 13: The spectra of D-T neutrons leaving the liquid metal for the models.

The number of neutrons leaving the lithium-lead was slightly lower than for the lithium, due to the increased shielding provided by the lead. The spectra show that the lithium-lead moderates the high energy neutrons much more than the lithium.

The larger the model the lower the fraction of neutrons that escape the liquid metal because the liquid metal has some shielding and internal scattering effect. More D-T neutrons escape the liquid metal than D-D neutrons due to their higher energies.

Having trace tritium or different impurities in the lithium had minimal effects on the spectra, those results are discussed in section 4.7.

4.4 Nuclide Inventory of the Liquid Metal

After the lifetime of the liquid metal (40 years), the dominant radionuclides that contribute to the activity of the liquid metal from 1 second to 1000 years after irradiation are shown in Figure 14, Figure 15 and Figure 16 for three of the large, D-T models: lithium with Supplier 1 impurities, lithium with Supplier 2 impurities and lithium-lead with Supplier 1 impurities. The activating neutrons were assumed to all be D-T neutrons, i.e. activation by D-D neutrons was not considered. These results are for an individual 'batch' of the liquid metal, i.e., 10% of the overall liquid metal.
The top two dominant radionuclides at each decay time are plotted. The plots for the other models are included in the appendix 7.7.

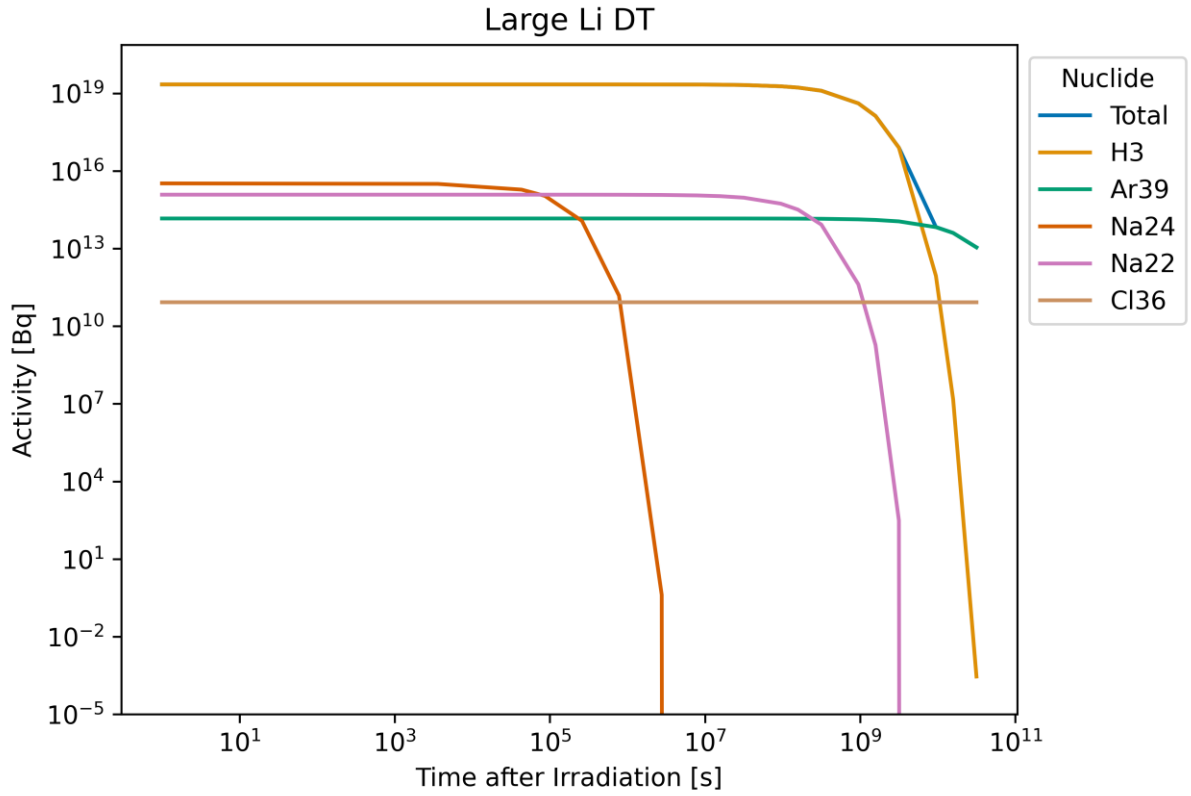

Figure 14: The dominant activity radionuclides for a batch of liquid metal for the large, D-T, lithium (Supplier 1) model.

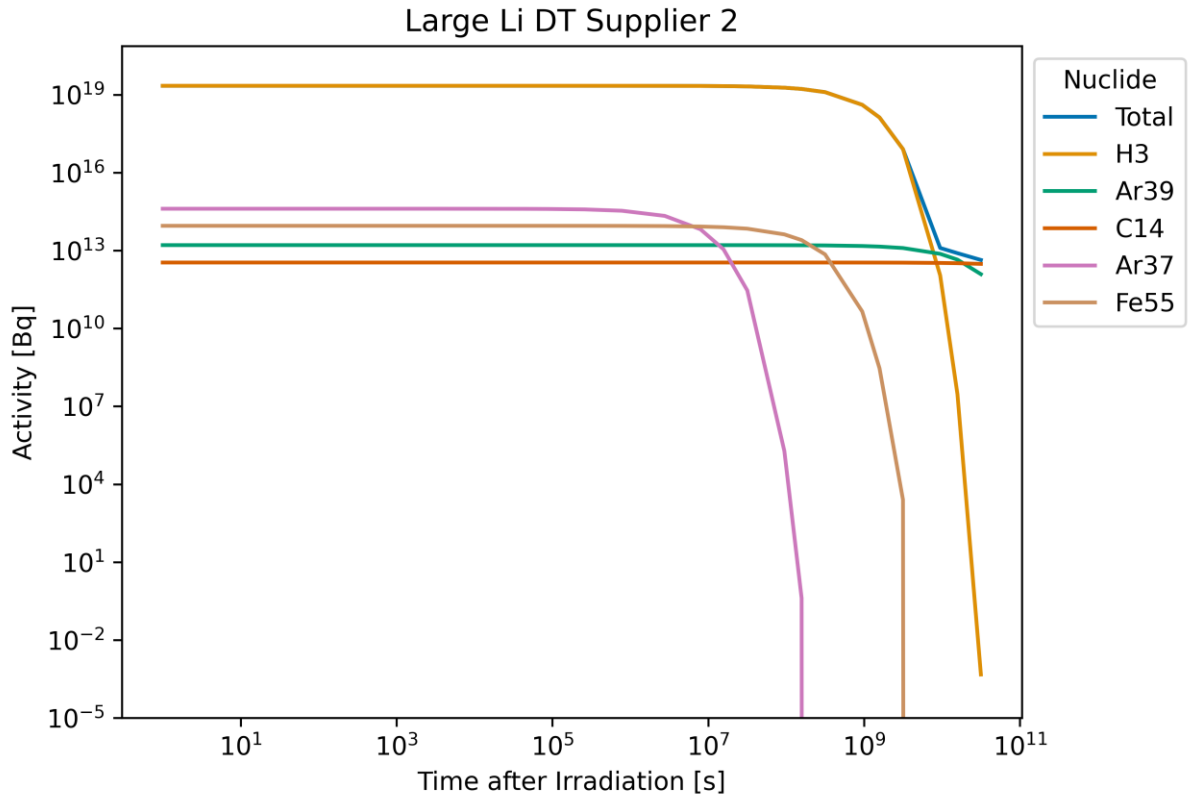

Figure 15: The dominant activity radionuclides for a batch of liquid metal for the large, D-T, lithium (Supplier 2) model.

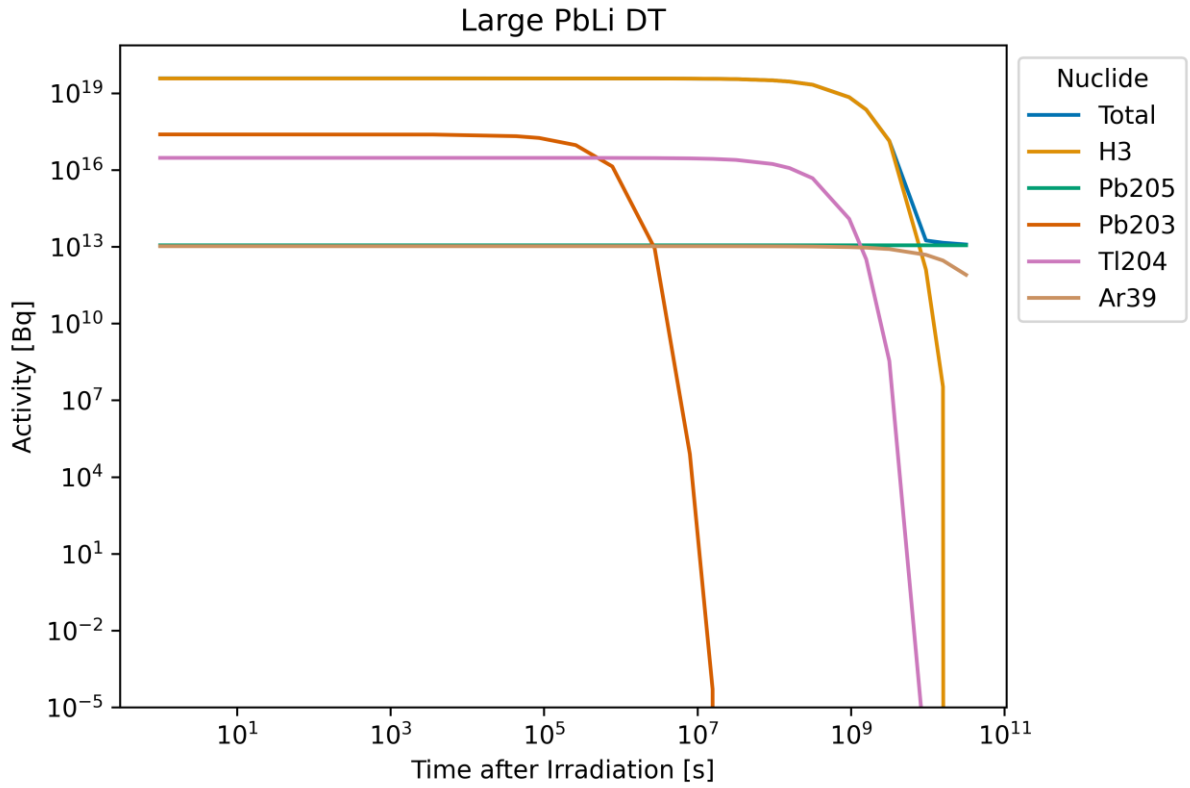

Figure 16: The dominant activity radionuclides for a batch of liquid metal for the large, D-T, lithium-lead (Supplier 1) model.

Detritiation was not considered in this analysis and so the activity of the liquid metals is dominated by tritium until it decays away after ~300 years (~10^9 seconds), where longer lived radionuclides take over, such as Ar-39.

The Supplier 2 impurities give different dominant radionuclides than the Supplier 1 ones, Ar-37, Fe-55 and C-14 are in the dominants' list instead of Na-24, Na-22 and Cl-36. However, the dominance of tritium is conserved.

For the lithium-lead results, Po-210 is present in the inventories. The maximum amounts of Po-210 in the inventories for the lithium-lead models is shown in Table 6.

Table 6: Maximum amounts of Po-210 in the lithium-lead inventories, for one 'batch'.

Model	Po-210 Mass [g]	Po-210 Activity [Bq]
Small D-T	21	3.5E+15
Nominal D-T	6.5	1.1E+15
Large D-T	2.6	4.4E+14

The equivalent plots are shown in Figure 17, Figure 18 and Figure 19 but for dominant bred masses rather than activity. Again, the plots for the other models are found in the appendix 7.8. The top 5 dominant nuclides at each decay time are plotted.

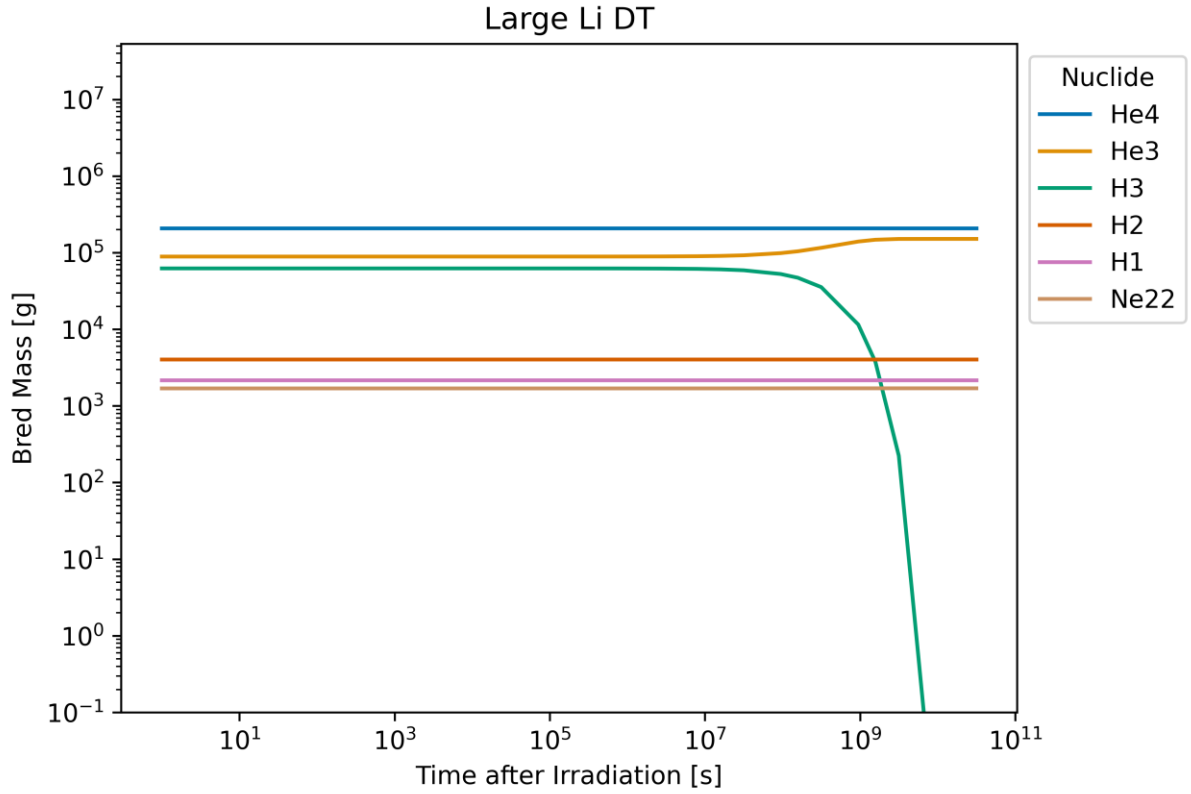

Figure 17: The dominant bred mass nuclides for a batch of liquid metal for the large, D-T, lithium (Supplier 1) model.

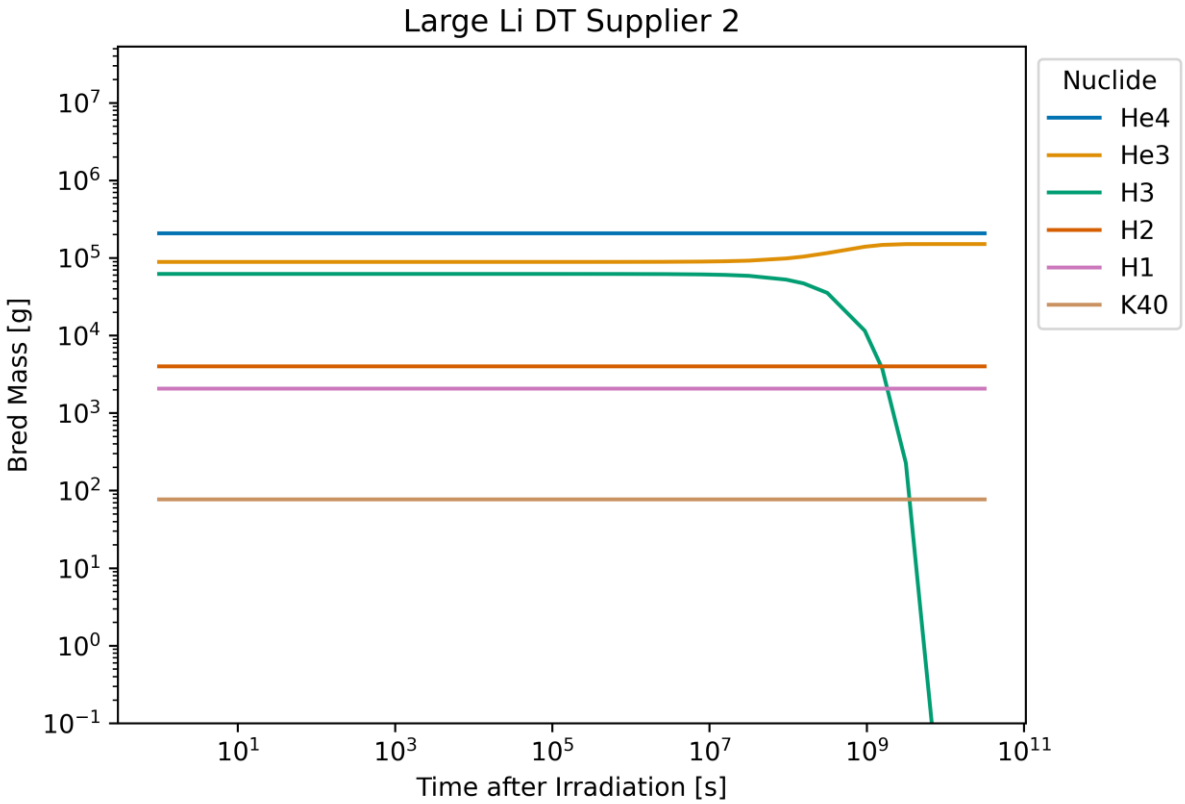

Figure 18: The dominant bred mass nuclides for a batch of liquid metal for the large, D-T, lithium (Supplier 2) model.

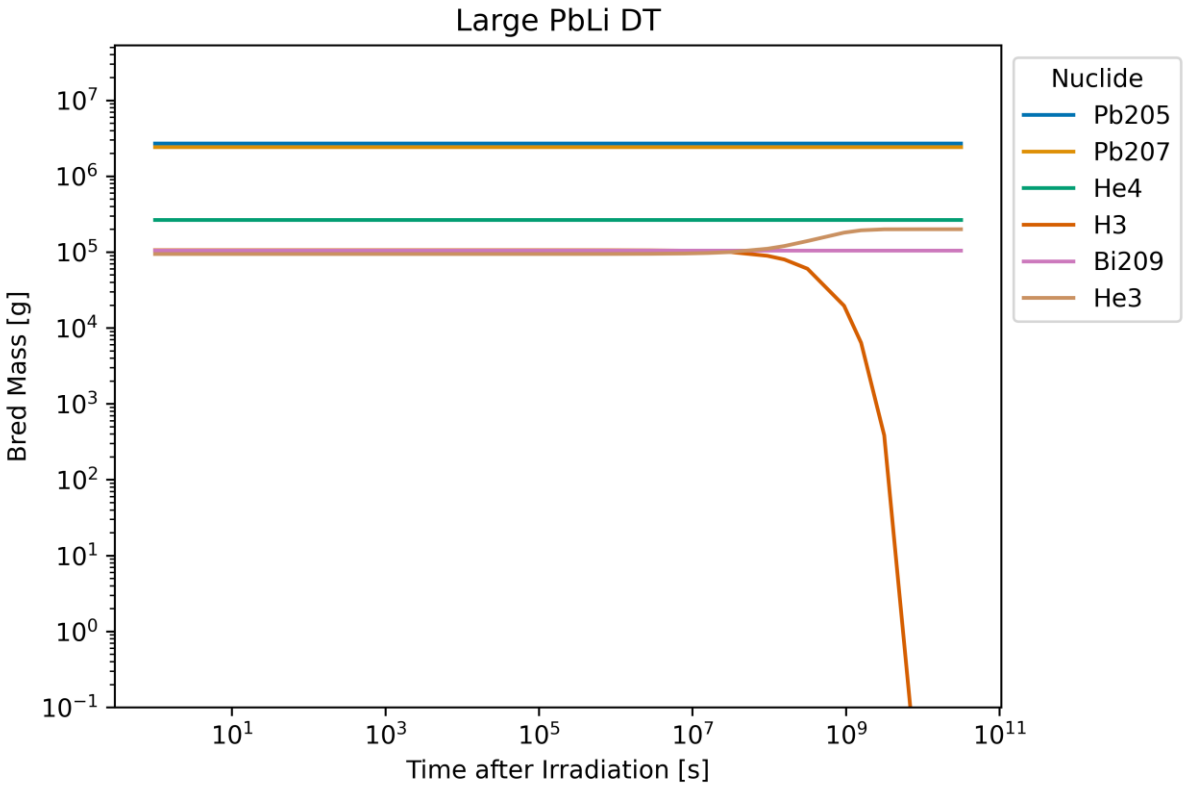

Figure 19: The dominant bred mass nuclides for a batch of liquid metal for the large, D-T, lithium-lead (Supplier 1) model.

From the dominant bred mass plots, the build-up of He-3 from the decay of tritium is observed. Detritiation was not considered in this analysis. Helium dominates the bred materials in the pure lithium models while the lithium-lead models are dominated by isotopes of lead. Note that these plots show only the bred material, i.e., the additional material not present initially in the liquid metal. For example, Pb-207 is present in natural lead, Figure 19 shows only the additional Pb-207 bred due to the irradiation.

Also included in the appendix 7.9 are the complete nuclide mass inventories 1 day after irradiation for the liquid metals in the models for reference which can be used to check for nuclides of interest. For example, Po-210 is present in the liquid-lead after irradiation. The largest amount of Po-210 occurs in the small, D-T model after 1 hour after irradiation when there is 21 g present which has an activity of 3.5E+15 Bq. The complete inventories for each decay time can be found in the accompanying json files.

The maximum Po-210 amount being in the small model is counterintuitive but is an artefact of the averaging of the flux used in the calculations and can be explained with the main pathway of the production:
Pb-208 (n, γ) Pb-209 (β- decay) Bi-209 (n, γ) Bi-210 (β- decay) Po-210.
The neutron source and thus the total number of neutrons is the same for the models and the volume of the lithium lead in the models is inherently different. Therefore, the average neutron flux over the small model is higher than for the large model. The number of Pb-208 atoms is higher in the large model than in the small model but these atoms experience the lower average flux in the large model. The differences in number of atoms and average neutron flux approximately cancel each other out and so approximately the same amount of Pb-209, and thus Bi-209, is produced in the models. The Bi-209 atoms then experience different average fluxes depending on the model size, producing more Bi-210, and thus Po-210, in the smaller model with the higher average flux.

Averaging the neutron flux over the volume of the material is a simplification because most of the reactions occur towards the inner radius where the neutron flux is highest (unless they are driven by thermal neutrons). The effect of this simplification is greater in larger volumes and for multi-step pathways. Therefore, the calculated amounts of Po-210 are underpredictions, especially in the large model.

4.5 Surrounding Structure Radiation Damage

The DPA values were calculated for the surrounding SS 316 structure for the different models over a 40-year lifetime. These results assumed all neutrons were D-T neutrons, they are plotted in Figure 20 and the values are included in the appendix 7.5.

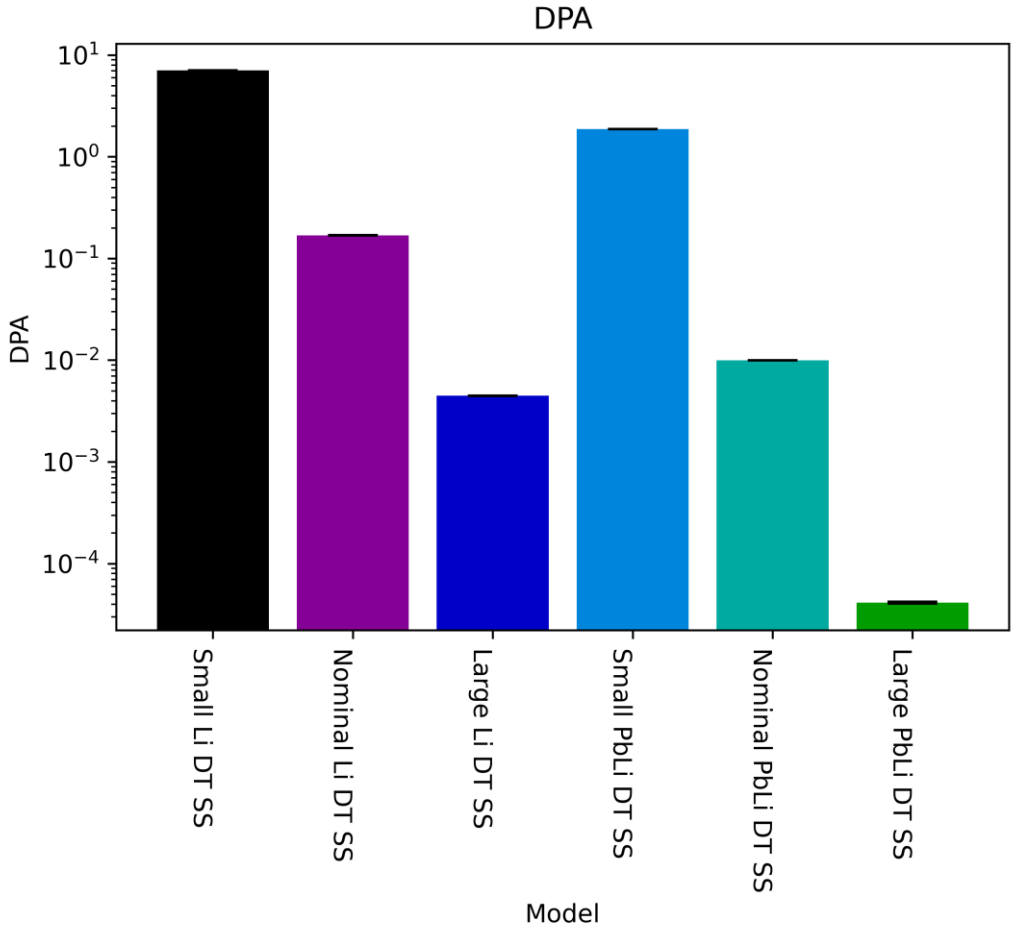

Figure 20: The DPA for the surrounding SS 316 structure over the 40-year lifetime for the different models.

The small models experience much higher DPA than the larger models and the pure lithium models experience more than the lithium-lead models. This is due to the extra shielding provided by the thicker liquid metal shells and the lithium-lead respectively. The maximum DPA calculated was 7 for the small, pure lithium, D-T model. For reference, some DPA values for nuclear devices are listed in Table 7.

Table 7: Reference DPA values for various nuclear devices [10].

Nuclear Device	**DPA**
LWR Fuel Cladding	20
Future Fast Reactors	150 – 200
Generation IV Reactors	~ 30 – 100
ITER	3
DEMO	~ 150

4.6 Surrounding Structure Activation

The activation of the surrounding SS 316 structure was calculated and compared to the Canadian and UK radioactive waste definitions. Since the waste limits use both volumetric and mass activity definitions, they were converted to absolute activity values using the volume and mass of the SS316 structure respectively. The activities and the dominant contributing radionuclides for the first 1000 years after shutdown for the large and small lithium models and the large lithium lead model are shown in Figure 21, Figure 22 and Figure 23, all were simulated with the D-T neutron source. The plots for the other models are

supplied in the appendix 7.6. The top two dominant radionuclides at each decay time are plotted. These results assume all neutrons are D-T neutrons.

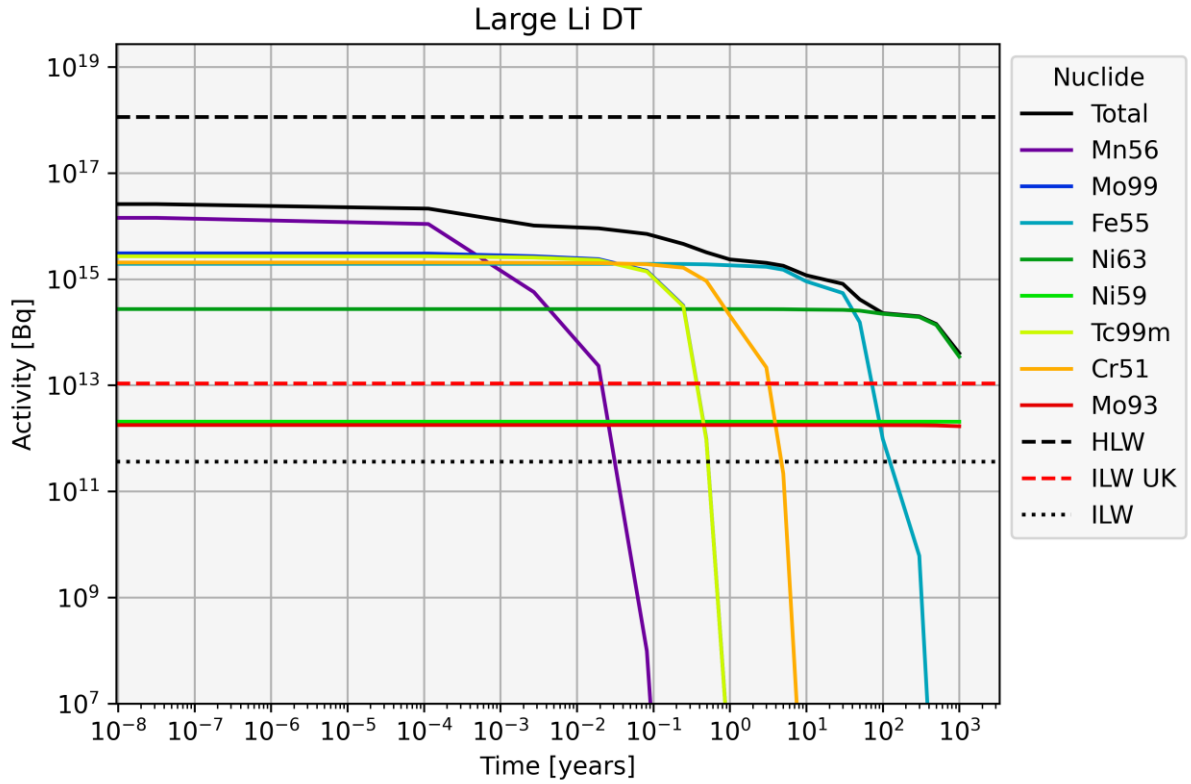

Figure 21: The activity and the dominant contributing radionuclides of the SS 316 surrounding structure for the large, lithium, D-T model for the first 1000 years after shutdown.

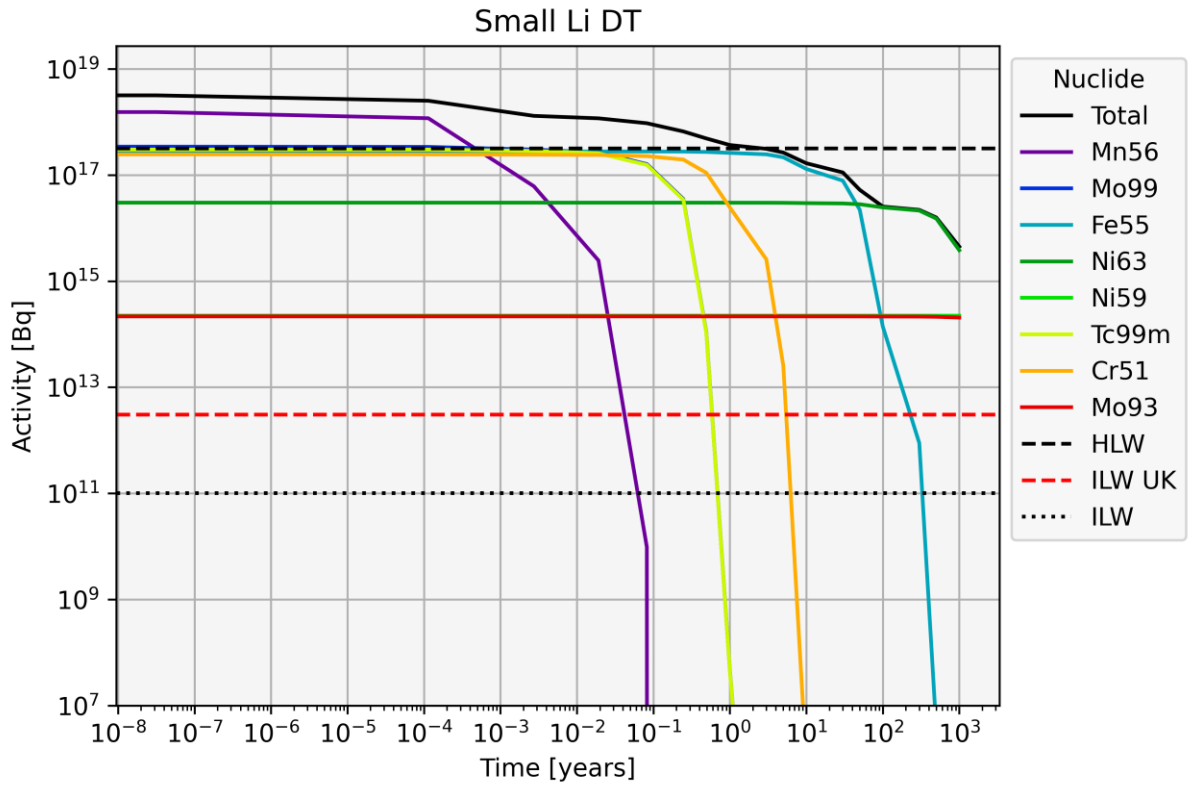

Figure 22: The activity and the dominant contributing radionuclides of the SS 316 surrounding structure for the small, lithium, D-T model for the first 1000 years after shutdown.

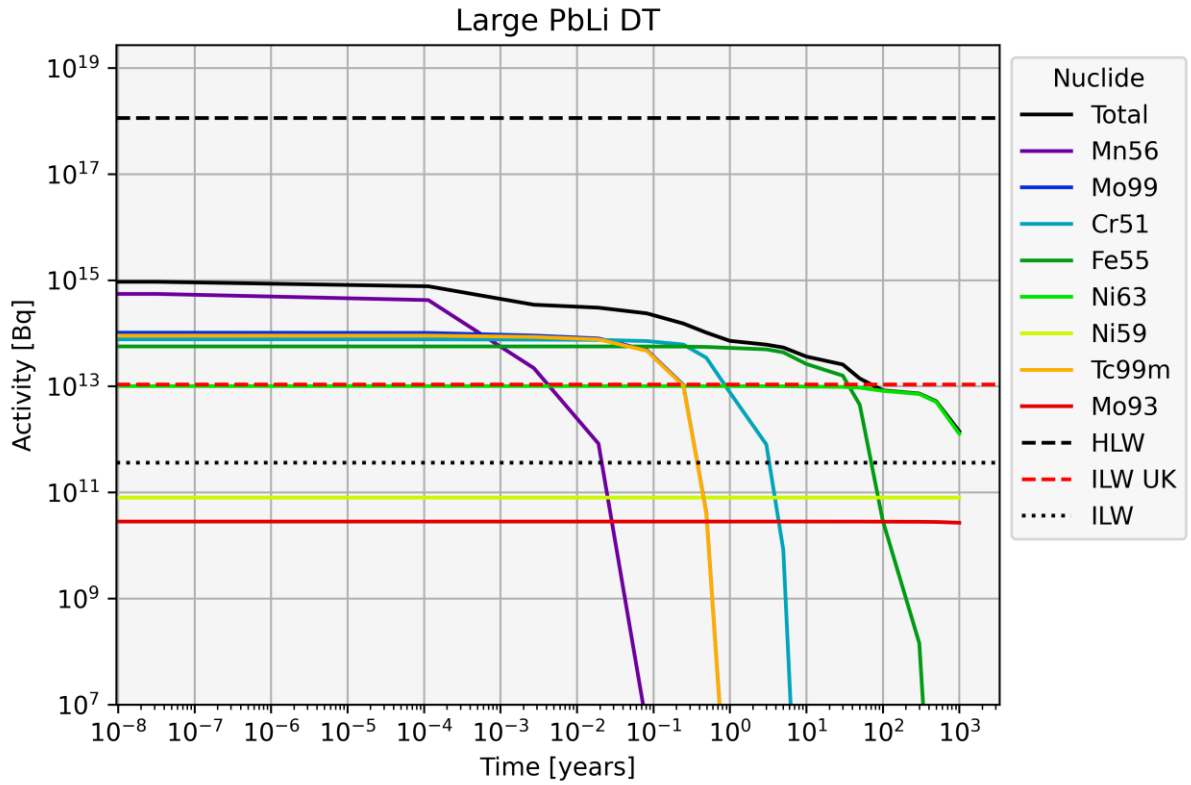

Figure 23: The activity and the dominant contributing radionuclides of the SS 316 surrounding structure for the large, lithium-lead, D-T model for the first 1000 years after shutdown.

From these three plots, the shielding effect from the liquid metal on the SS 316 structure is shown. The thicker liquid metal layer provides more shielding and so there is less activation in the SS 316, also the lithium-lead provides more shielding than lithium and again there is less activation in the SS 316.7.6

The activation of the small, lithium model shown in Figure 22 is high and falls below the HLW threshold after about 2 years.

Both large models never have HLW and can be immediately considered for long-term ILW management. However, the short-term heat generation may still require some initial, heat-dissipating containment. The same result is observed for the nominal-sized models (see appendix 7.6).

The dominant radionuclide in ILW after 1000 years for all models was nickel-63 with a half-life of 100 years. This is a long-lived beta emitter for which the Canadian LLW limits can be considerably higher depending on the site and disposal facility. Therefore, there is a possibility that the SS 316 structure will be admissible as LLW sooner than this conservative analysis predicts. The other dominant long-lived radioisotopes for the models are nickel-59 (half-life 76000 years) and molybdenum-93 (half-life 4800 years). These radioisotopes decay via electron-capture and produce low-energy gamma rays and so may also be subject to higher Canadian LLW limits.

The main pathways for the dominant contributing radionuclides are as follows:

- Mn55 (n, gamma) Mn56
- Mo98 (n, gamma) Mo99
- Fe54 (n, gamma) Fe55
- Ni62 (n, gamma) Ni63
- Ni58 (n, gamma) Ni59
- Mo98 (n, gamma) Mo99 (β- decay) Tc99m

- Cr50 (n, gamma) Cr51
- Mo92 (n, gamma) Mo93

From an activation perspective, SS 316 could be replaced with a lower-activation material that avoids or reduces the amounts of the above listed isotopes to reduce the activation of the structure.

4.7 Trace Tritium and different Impurities

Trace tritium due to tritium cycle inefficiencies were added to the large, lithium, D-T model. The results due to this addition are included in Figure 5 and

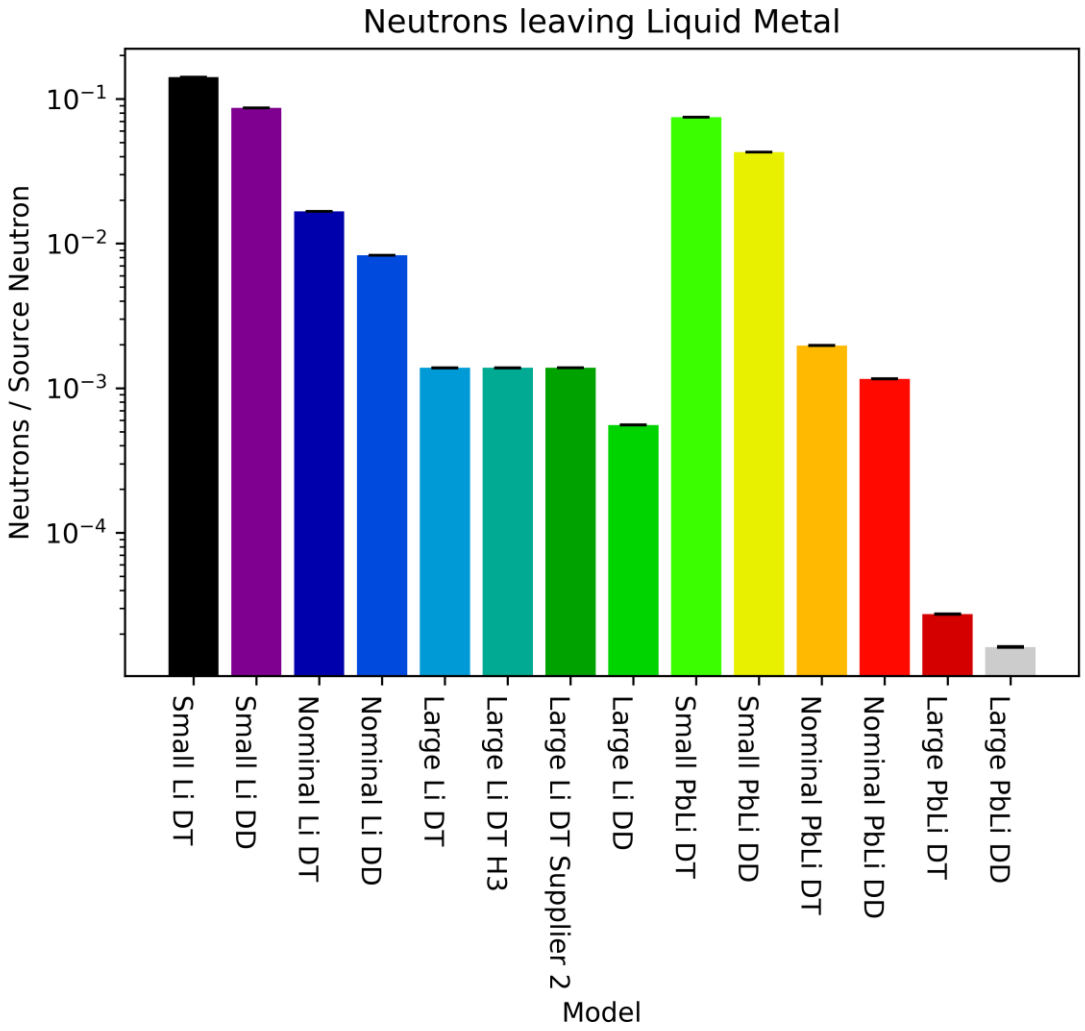

Figure 11. Different lithium impurities were added to the large, lithium, D-T model. The results due to this change are included in Figure 5,

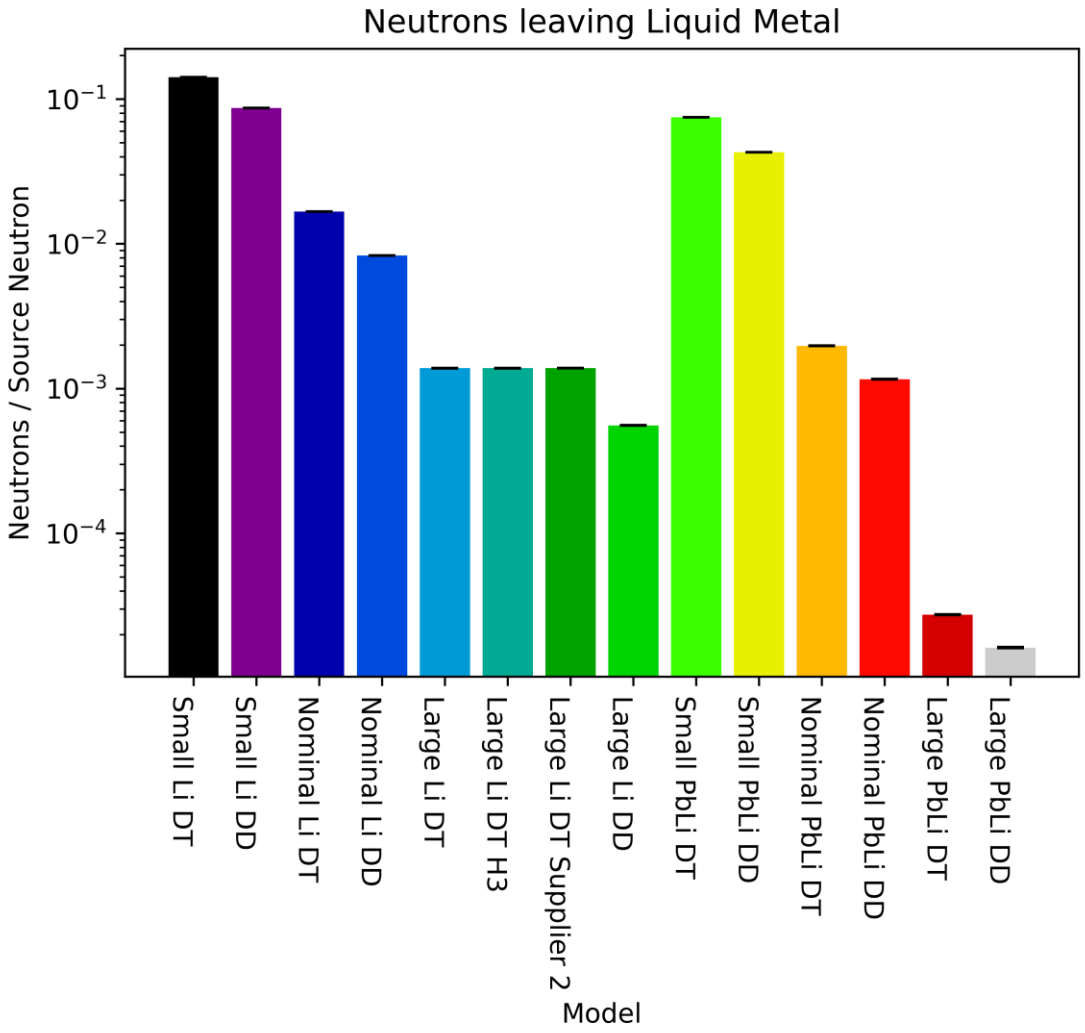

Figure 11, Figure 15 and Figure 18.

Both of these changes to the liquid lithium composition had very minimal effects on the results. In fact, these results were omitted from the line plots (Figure 7, Figure 10 and Figure 13) because they were indistinguishable from one another and also the standard large, lithium, D-T model results. The ratio between these results for the line plots are shown in Figure 24, Figure 25 and Figure 26. The ratios are all very close to unity showing that there was very little effect in altering the lithium composition.

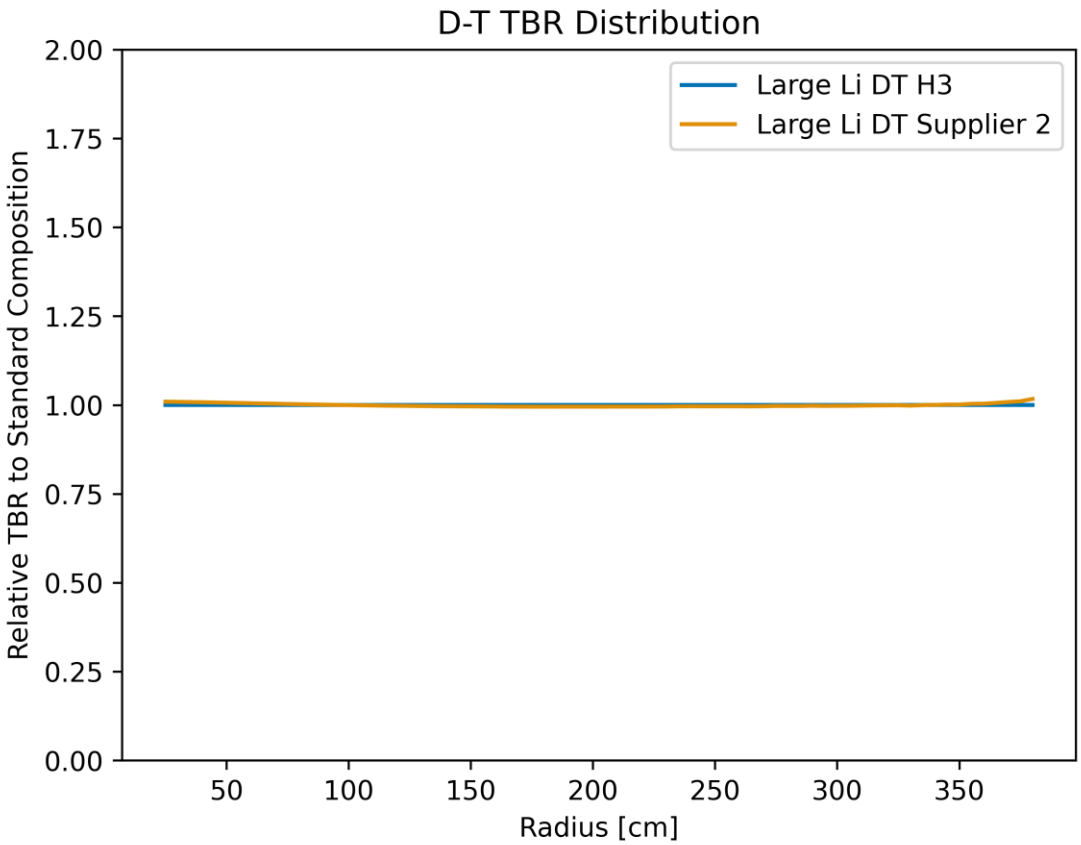

Figure 24: Ratio of TBR in the modified lithium compositions to the standard composition.

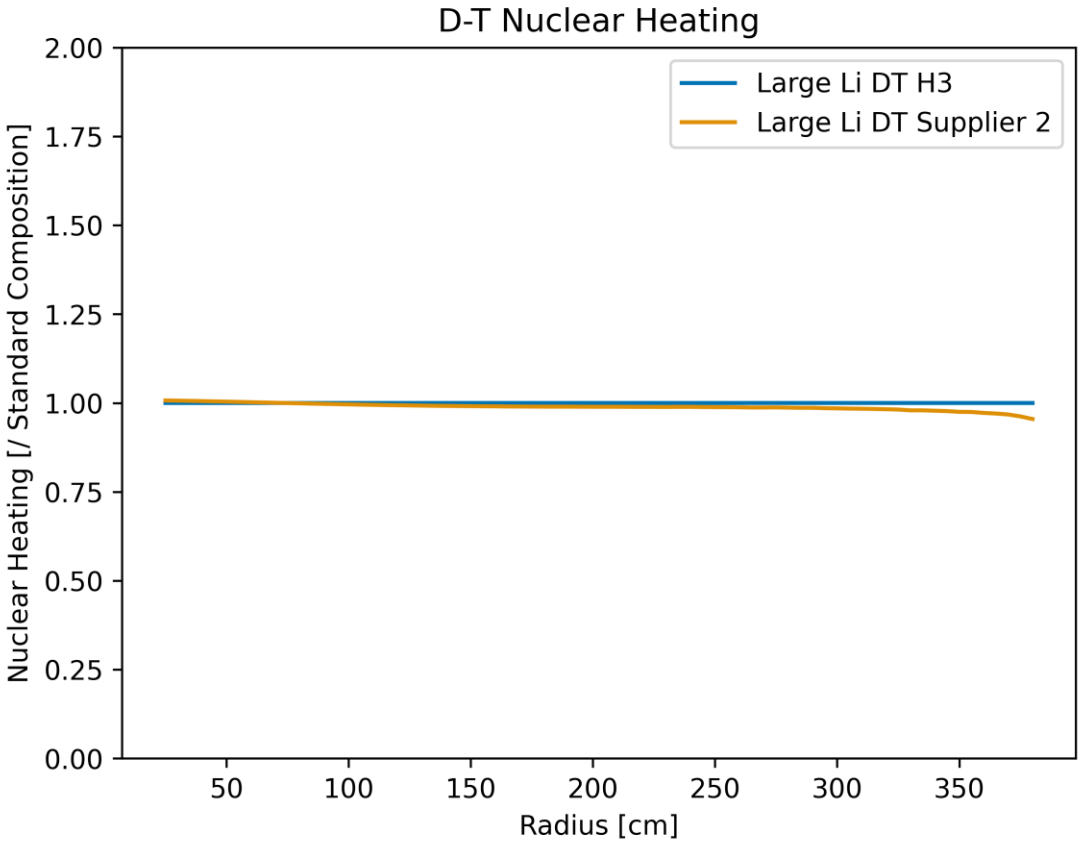

Figure 25: Ratio of nuclear heating in the modified lithium compositions to the standard composition.

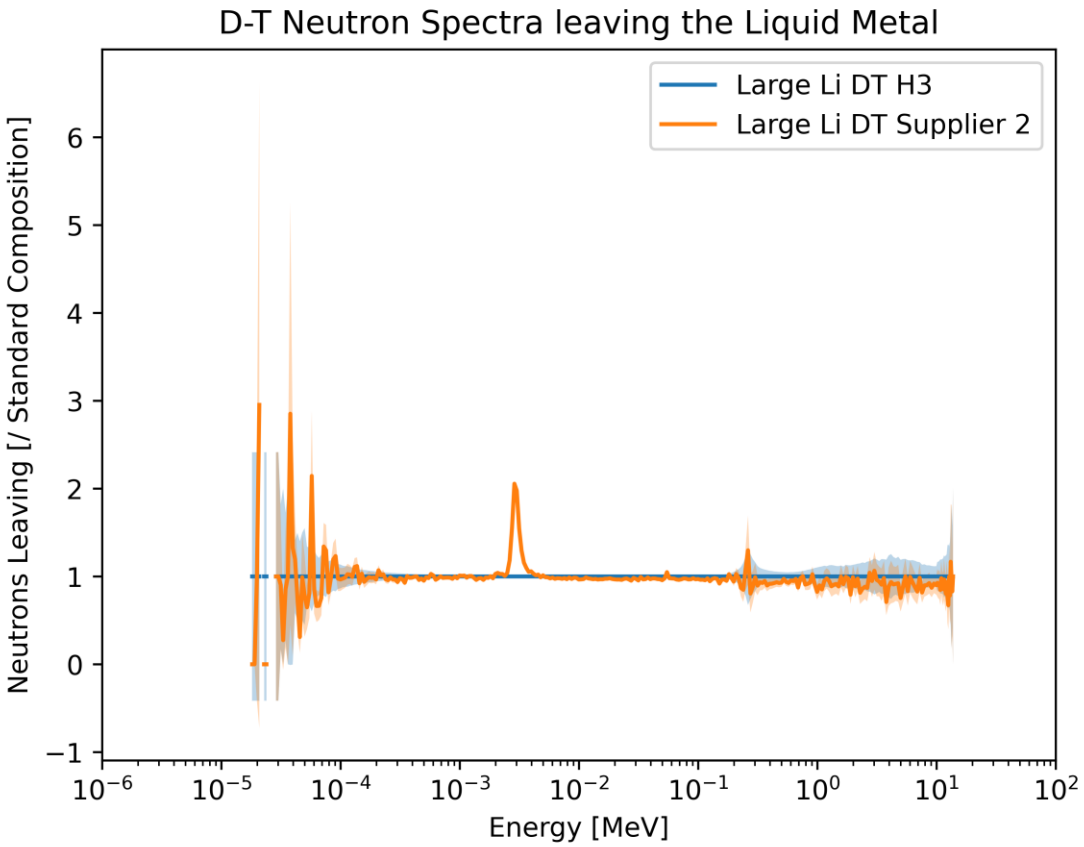

Figure 26: Ratio of neutron spectra leaving the lithium with modified compositions to the standard composition.

5 CONCLUSION

Preliminary TBR analysis was performed on a spherical model with parameters representative of General Fusion's MTF concept with basic assumptions. Nuclear responses of the breeder material were calculated including: tritium production, nuclear heating, leakage neutrons and nuclide inventory. Analysis on a simplified representation of the surrounding structure was also performed. Radiation damage and activation of this structure was calculated. Different concept models were analysed including varied sizes, breeder materials and breeder impurities.

The relative results between different models were generally affected by the extra shielding provided by the larger geometries and the lithium-lead breeder over the lithium breeder. High TBR values were calculated for D-T neutrons of greater than 1.5. The TBR values for the models simulating D-T neutrons are shown in Table 8.

Table 8: The TBR values calculated for the different models using the D-T reaction.

DT Model	TBR (± statistical uncertainty)
Small Li	1.73 ± 0.00
Nominal Li	1.86 ± 0.00
Large Li	1.87 ± 0.00
Large Li H3	1.87 ± 0.00
Large Li Supplier 2	1.88 ± 0.00
Large Li SS	1.88 ± 0.00
Small PbLi	1.58 ± 0.00
Nominal PbLi	1.65 ± 0.00
Large PbLi	1.65 ± 0.00

Activation inventories of the liquid metals were calculated. Lithium-lead inventories contained Po-210, the maximum being in the small, D-T model where there was 21 g present with an activity of 3.5E+15 Bq.

The radiation-induced DPA damage in the SS structure in the models with the least intrinsic shielding is on the same order as other nuclear machines worldwide. These models with low intrinsic shielding (i.e., small with lithium breeder) were calculated to generate HLW in the SS structure that remains for the order of years after shutdown of the machine. The Nominal and Large models were calculated to generate no HLW in the SS structure but may require some initial heat-dissipating containment. SS 316 was used in this analysis, replacing this with a lower-activation material would reduce the activation levels.

6 REFERENCES

[1] M. Wight, “Statement of Work for Tritium Breeding and Neutron Shielding in Lithium SP-000214 Rev 0,” General Fusion, 2023.

[2] D. Krotez, “Personal communication 16/12/2023”.

[3] M. Jakobs, “Fusion Energy - Burning Questions,” 2016.

[4] G. Bailey, D. Foster, P. Kanth and M. Gilbert, “The FISPACT-II User,” UKAEA-CCFE-RE(21)02, Available from http://fispact.ukaea.uk, May 2021.

[5] AZO Materials, “Grade 316 Stainless Steel: Properties, Fabrication and Applications,” AZO Materials, 18 May 2005. [Online]. Available: https://www.azom.com/article.aspx?ArticleID=2868. [Accessed 03 January 2024].

[6] A. Y. Konobeyev, “DPA cross-section data for SS-316 prepared using standard NRT model,” KIT, 2013.

[7] Canadian Nuclear Safety Commission, “Canadian National Report for the Joint Convention on the Safety of Spent Fuel Management and on the Safety of Radioactive Waste Management,” 2020.

[8] Uk Gov, “The Environmental Permitting (England and Wales) Regulations 2016: SCHEDULE 23 Radioactive substance activities,” 2016.

[9] L. A. El-Guebaly and S. Malang, “Toward the ultimate goal of tritium self-sufficiency: Technical issues and requirements imposed on ARIES advanced power plants,” *Fusion Engineering and Design,* vol. 84, no. 12, pp. 2072-2083, 2009.

[10] IAEA, “Development of Radiation Resistant Reactor Core Structural Materials,” 2007.

7 APPENDIX

7.1 Pulse Approximation

Two approaches for modelling the pulses are shown for the large, lithium-lead D-D model. Both average the pulses over the 40 year lifetime except for a short period at the end. In Figure 27 the pulses averaged over each cycle for the last 5 days of the lifetime. In Figure 28 the pulses are modelled accurately for the last cycle (220 s) of the lifetime. The figures show that even though the 5 day plot averages the pulses, it allows enough time for the short-lived products, particularly Pb-209 (half-life 3 hours), to build up, whereas the 220 second plot doesn't. The long-lived products are unchanged.

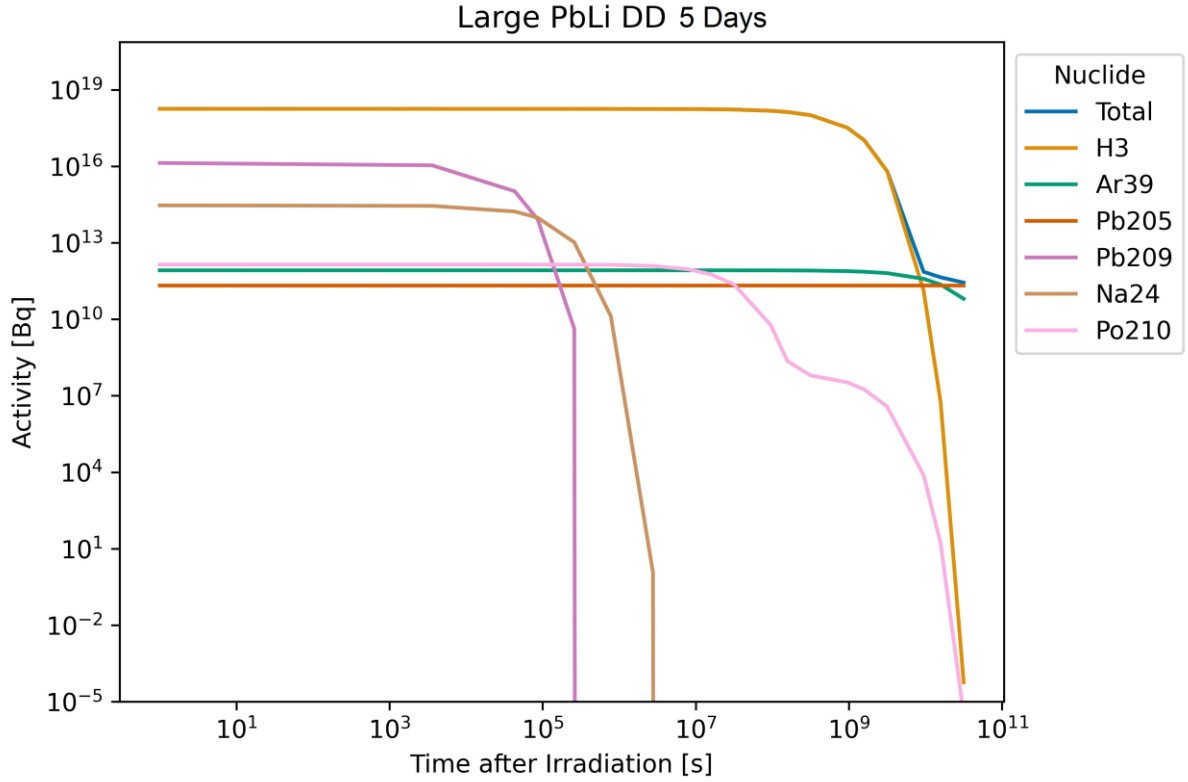

Figure 27: The dominant activity radionuclides for a batch of liquid metal for the large, D-D, lithium-lead model, including modelling the cycles of the last 5 days of the lifetime.

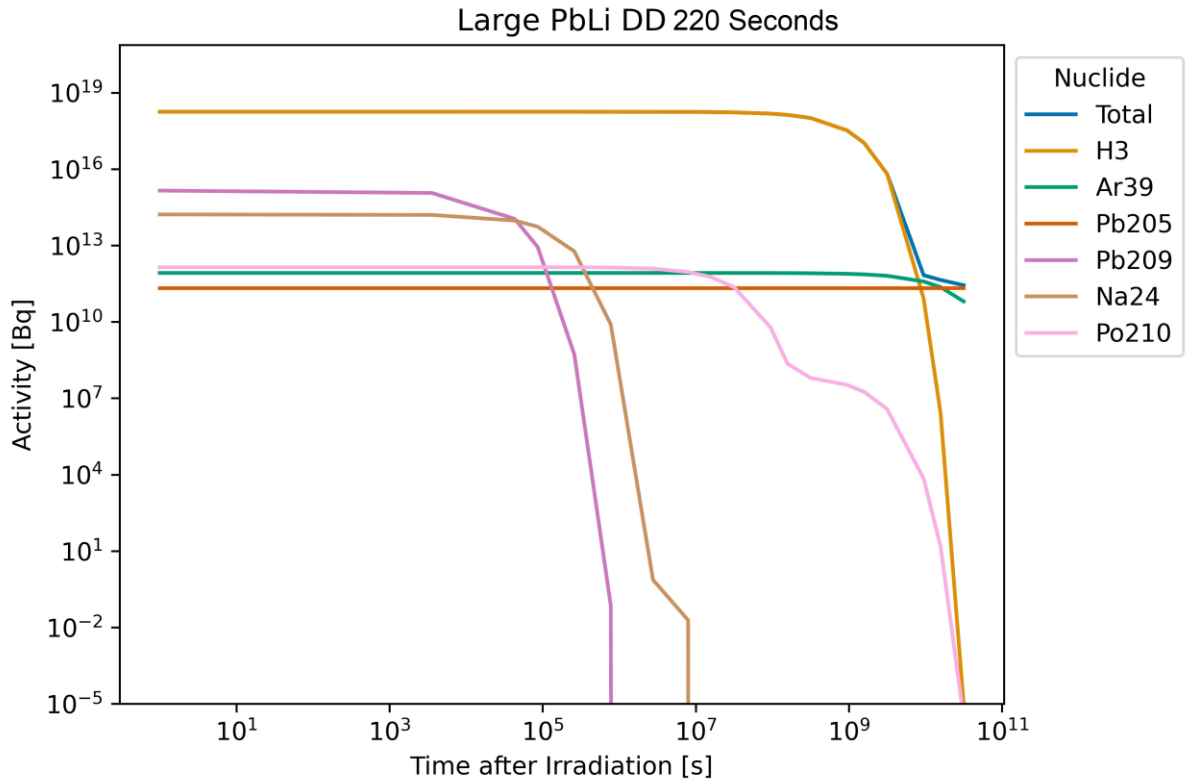

Figure 28: The dominant activity radionuclides for a batch of liquid metal for the large, D-D, lithium-lead model, including modelling the pulses of the last cycle (220 s) of the lifetime.

7.2 Tritium Production

Table 9: Tritium production per fusion reaction for the different models.

Model	Tritium production per fusion reaction	Statistical Uncertainty
Small Li DT	1.732	0
Small Li DD	0.912	0
Nominal Li DT	1.859	0
Nominal Li DD	0.991	0
Large Li DT	1.875	0
Large Li DT H3	1.875	0
Large Li DT Supplier 2	1.880	0
Large Li DT SS	1.876	0
Large Li DD	0.999	0
Large Li DD SS	0.999	0
Small PbLi DT	1.579	0
Small PbLi DD	0.829	0
Nominal PbLi DT	1.646	0
Nominal PbLi DD	0.868	0
Large PbLi DT	1.648	0
Large PbLi DD	0.869	0

7.3 Nuclear Heating

Table 10: Nuclear heating in the liquid metal per fusion reaction.

Model	Nuclear Heating per fusion reaction [MeV]	Statistical Uncertainty
Small Li DT	1.553E+01	2E-02
Small Li DD	6.80E+00	2E-02
Nominal Li DT	1.619E+01	3E-02
Nominal Li DD	7.19E+00	2E-02
Large Li DT	1.627E+01	3E-02
Large Li DT SS	1.628E+01	3E-02
Large Li DD	7.23E+00	2E-02
Small PbLi DT	1.584E+01	2E-02
Small PbLi DD	6.92E+00	3E-02
Nominal PbLi DT	1.619E+01	3E-02
Nominal PbLi DD	7.12E+00	3E-02
Large PbLi DT	1.620E+01	3E-02
Large PbLi DD	7.12E+00	3E-02

7.4 Leakage Neutrons

Table 11: Fraction of source neutrons leaving the liquid metal for each model.

Model	Fraction of source neutrons leaving liquid metal	Statistical Uncertainty
Small Li DT	1.4183E-01	1E-05
Small Li DD	8.6870E-02	9E-06
Nominal Li DT	1.6707E-02	3E-06
Nominal Li DD	8.280E-03	2E-06
Large Li DT	1.382E-03	1E-06
Large Li DT H3	1.382E-03	1E-06
Large Li DT Supplier 2	1.383E-03	1E-06
Large Li DD	5.568E-04	6E-07
Small PbLi DT	7.4759E-02	7E-06
Small PbLi DD	4.2895E-02	4E-06
Nominal PbLi DT	1.973E-03	1E-06
Nominal PbLi DD	1.1599E-03	9E-07
Large PbLi DT	2.74E-05	1E-07
Large PbLi DD	1.62E-05	1E-07

7.5 Surrounding Structure Radiation Damage

Table 12: DPA in the SS structures.

Model	DPA	Statistical Uncertainty
Small Li DT SS	7.1E+00	1E-03
Nominal Li DT SS	1.7E-01	1E-04
Large Li DT SS	4.5E-03	1E-05
Small PbLi DT SS	1.9E+00	5E-04
Nominal PbLi DT SS	1.0E-02	2E-05
Large PbLi DT SS	4.1E-05	9E-07

7.6 Surrounding Structure Activation

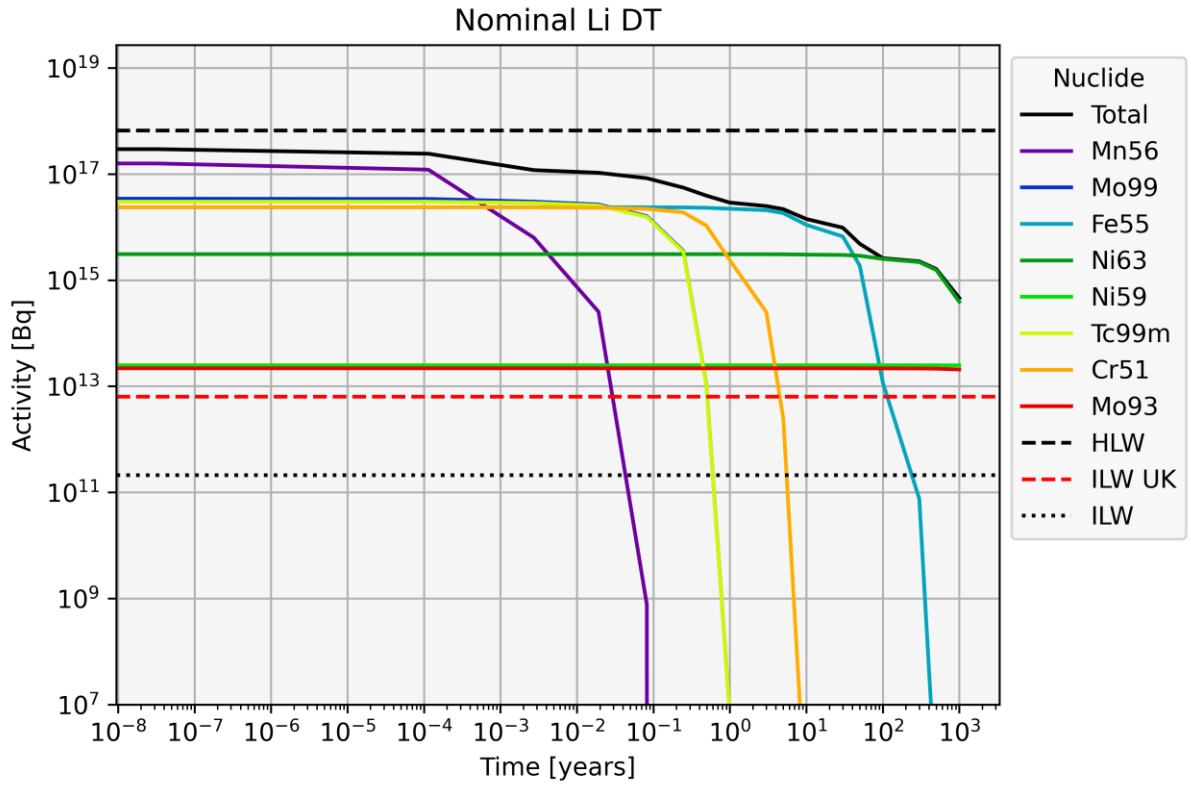

Figure 29: The activity and the dominant contributing radionuclides of the SS 316 surrounding structure for the nominal, lithium, D-T model for the first 1000 years after shutdown.

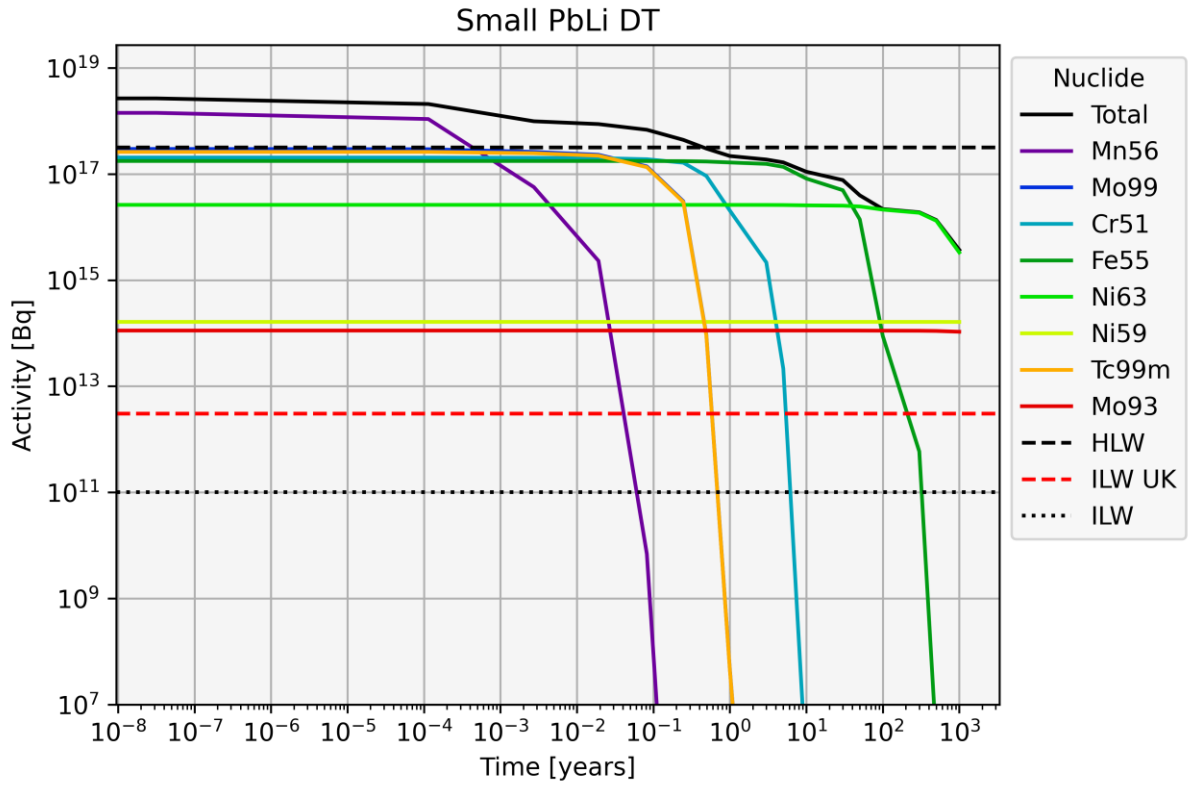

Figure 30: The activity and the dominant contributing radionuclides of the SS 316 surrounding structure for the small, lithium-lead, D-T model for the first 1000 years after shutdown.

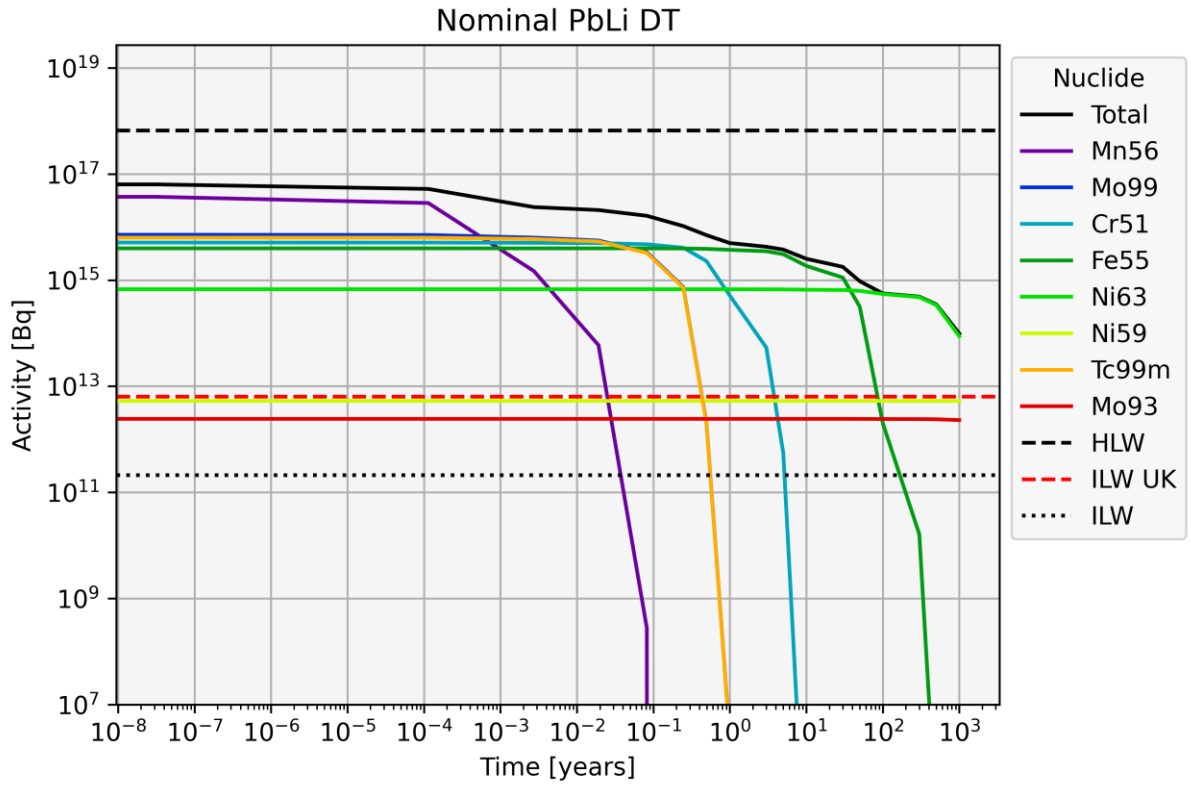

Figure 31: The activity and the dominant contributing radionuclides of the SS 316 surrounding structure for the nominal, lithium-lead, D-T model for the first 1000 years after shutdown.

7.7 Nuclide inventory of the Liquid Metal (activities) (plots)

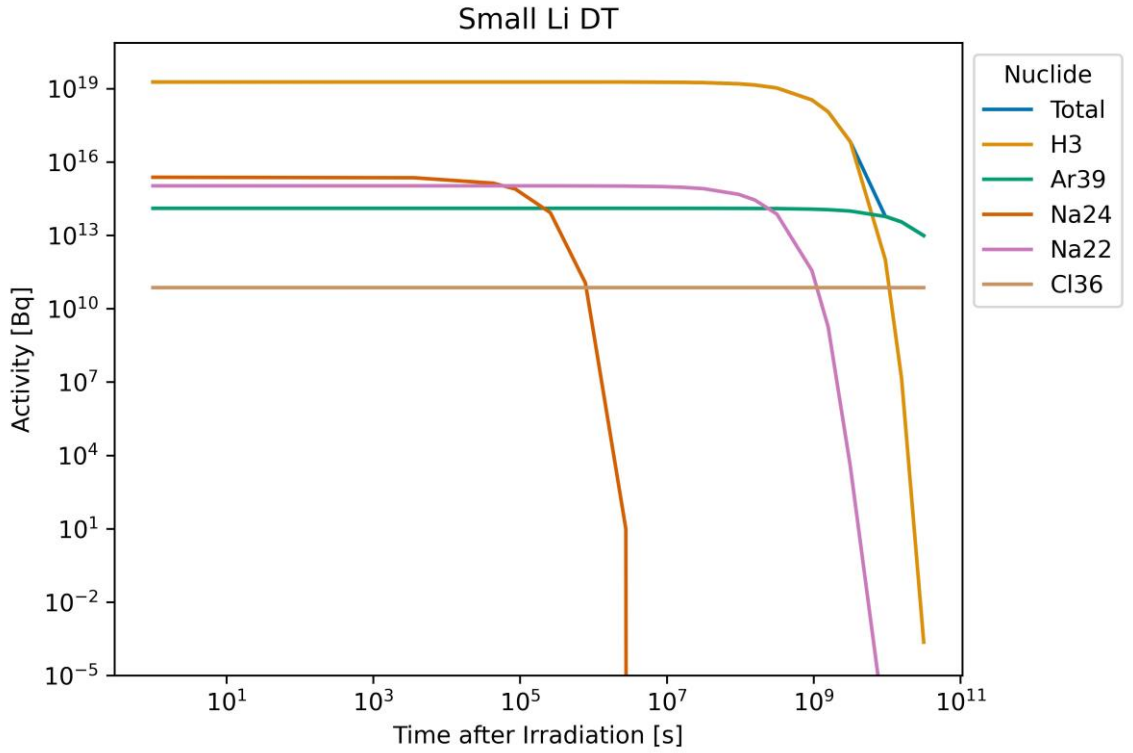

Figure 32: The dominant activity radionuclides for a batch of liquid metal for the small, D-T, lithium model.

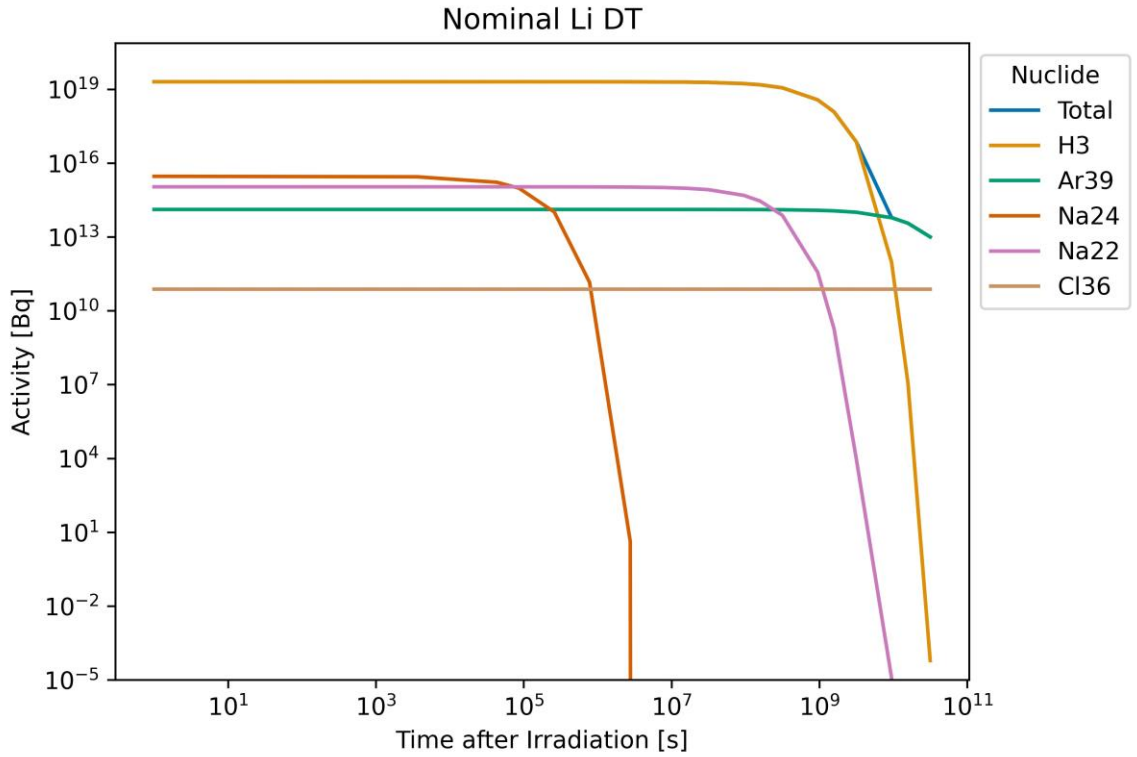

Figure 33: The dominant activity radionuclides for a batch of liquid metal for the nominal, D-T, lithium model.

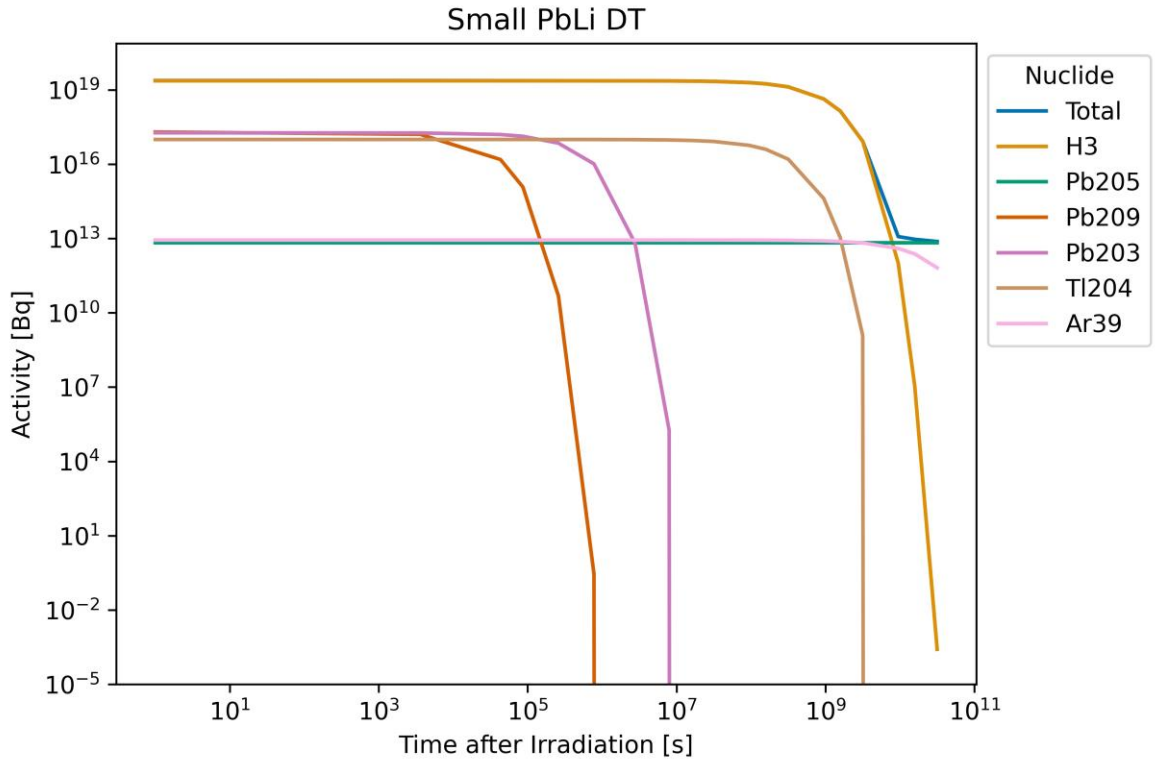

Figure 34: The dominant activity radionuclides for a batch of liquid metal for the small, D-T, lithium-lead model.

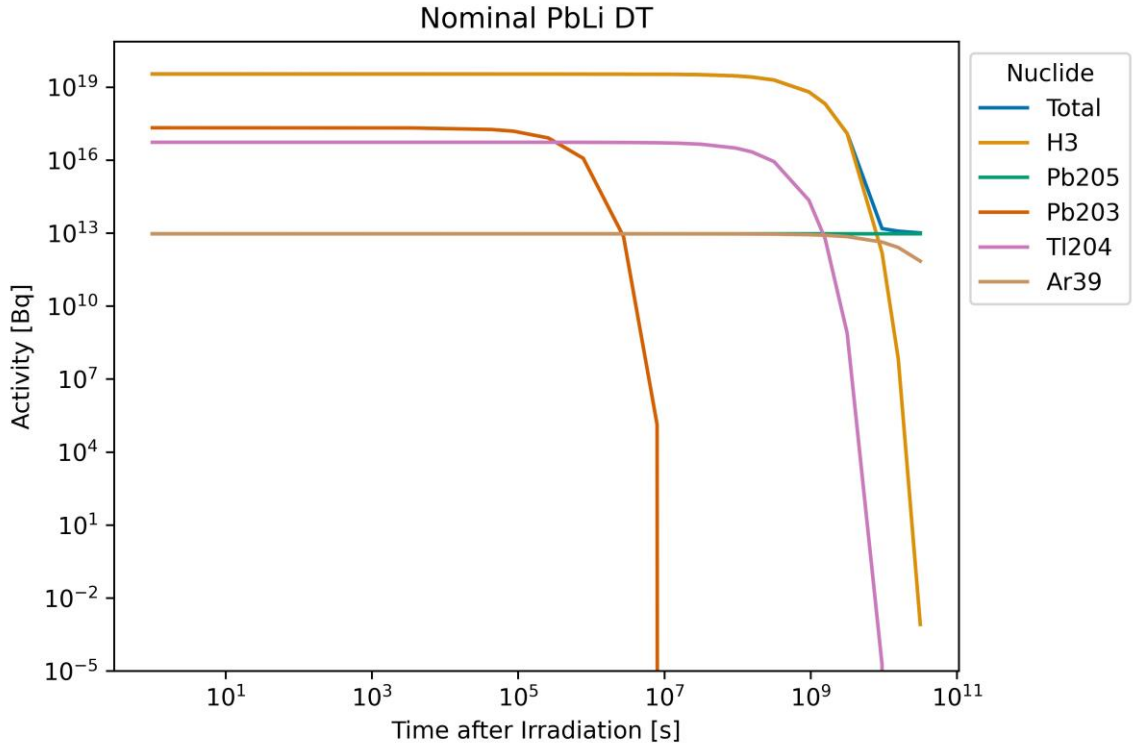

Figure 35: The dominant activity radionuclides for a batch of liquid metal for the nominal, D-T, lithium-lead model.

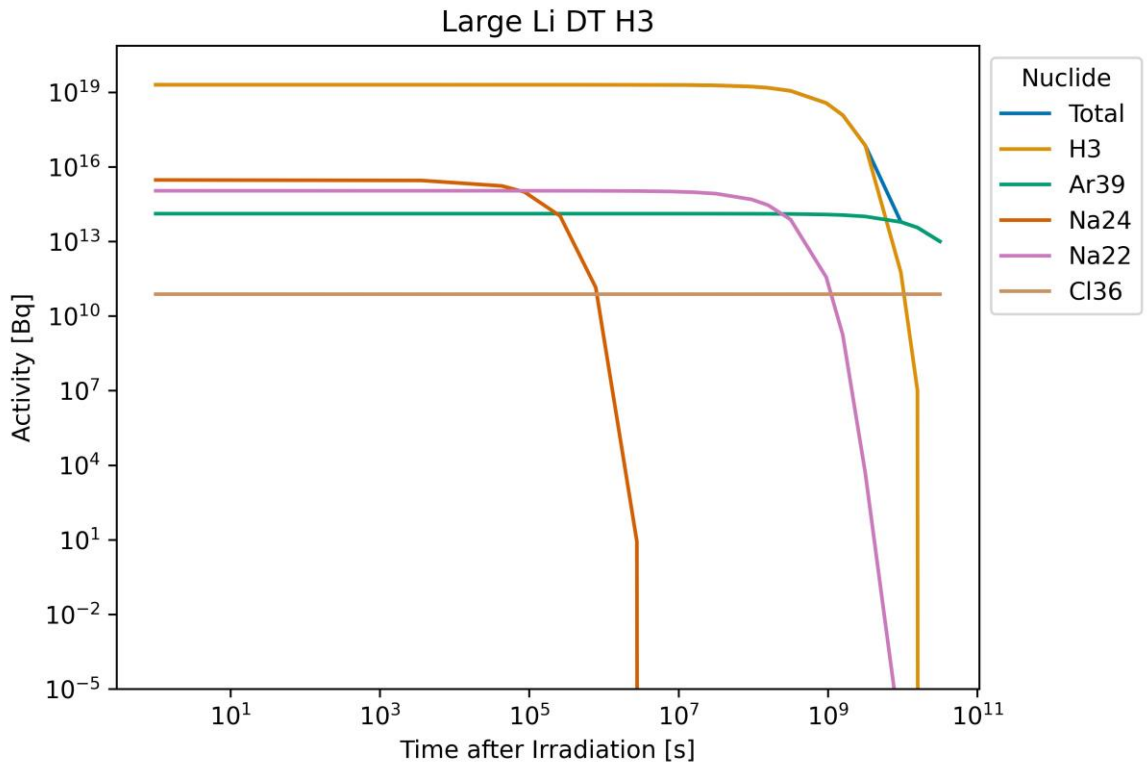

Figure 36: The dominant activity radionuclides for a batch of liquid metal for the large, D-T, lithium model with trace tritium in the initial inventory.

7.8 Nuclide Inventory of the Liquid Metal (masses) (plots)

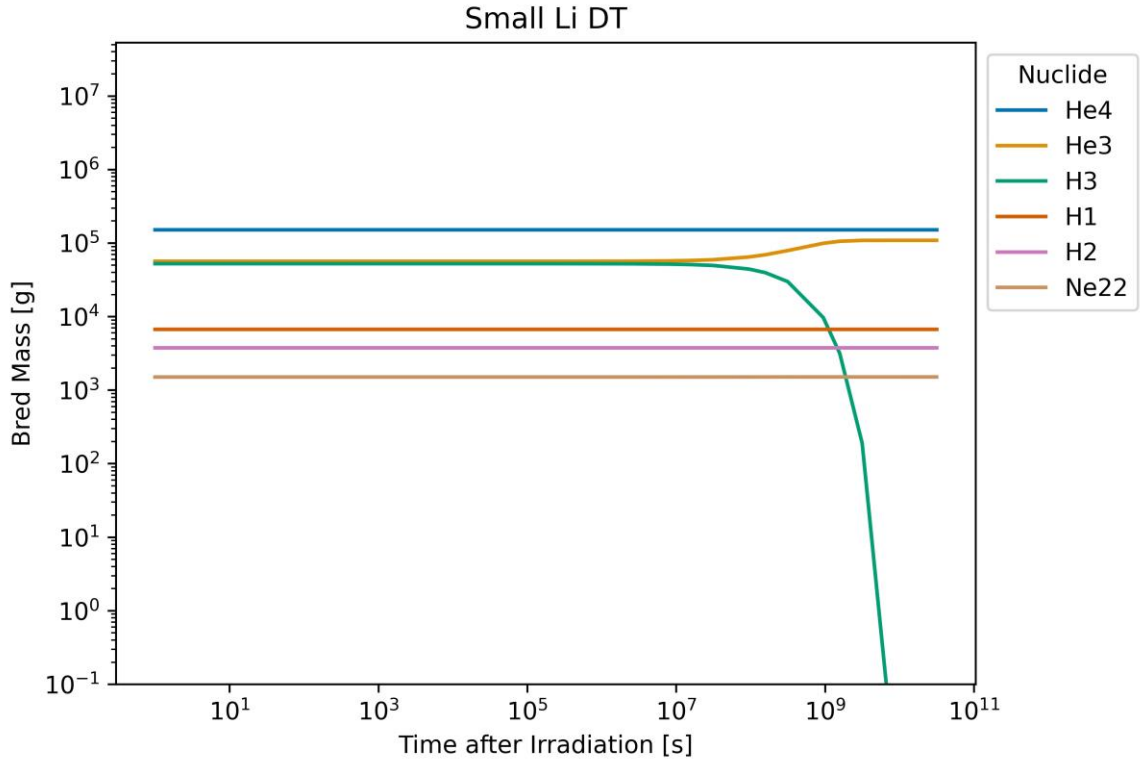

Figure 37: The dominant bred mass nuclides for a batch of liquid metal for the small, D-T, lithium model.

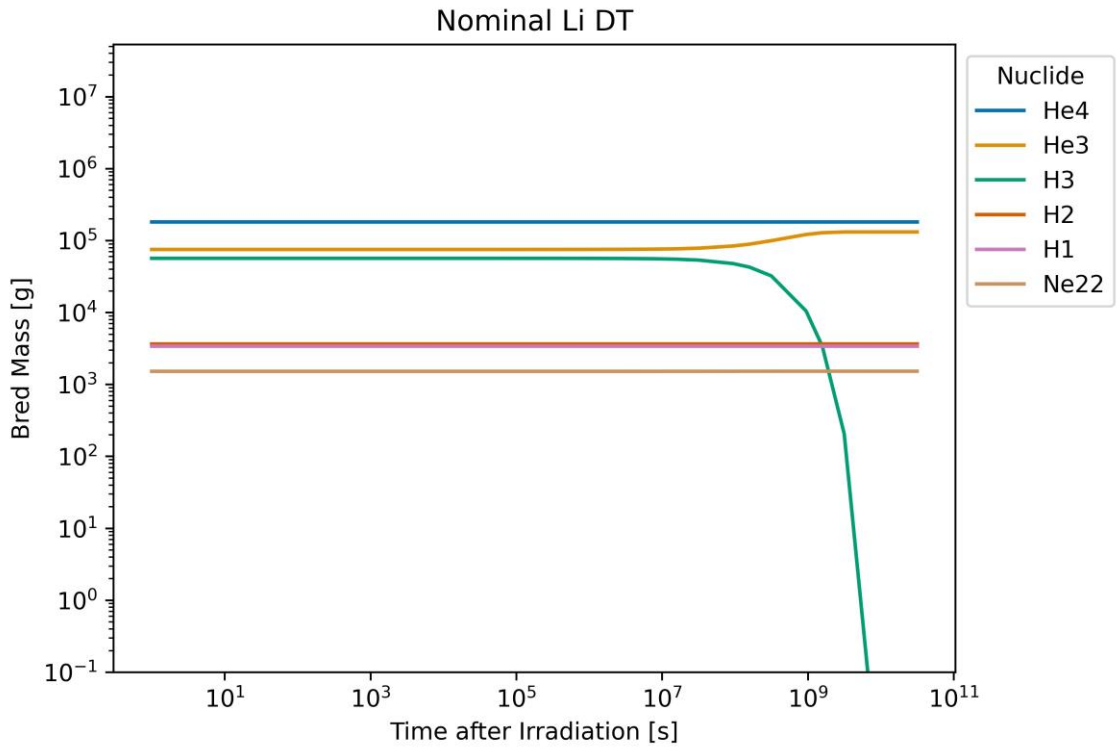

Figure 38: The dominant bred mass nuclides for a batch of liquid metal for the nominal, D-T, lithium model.

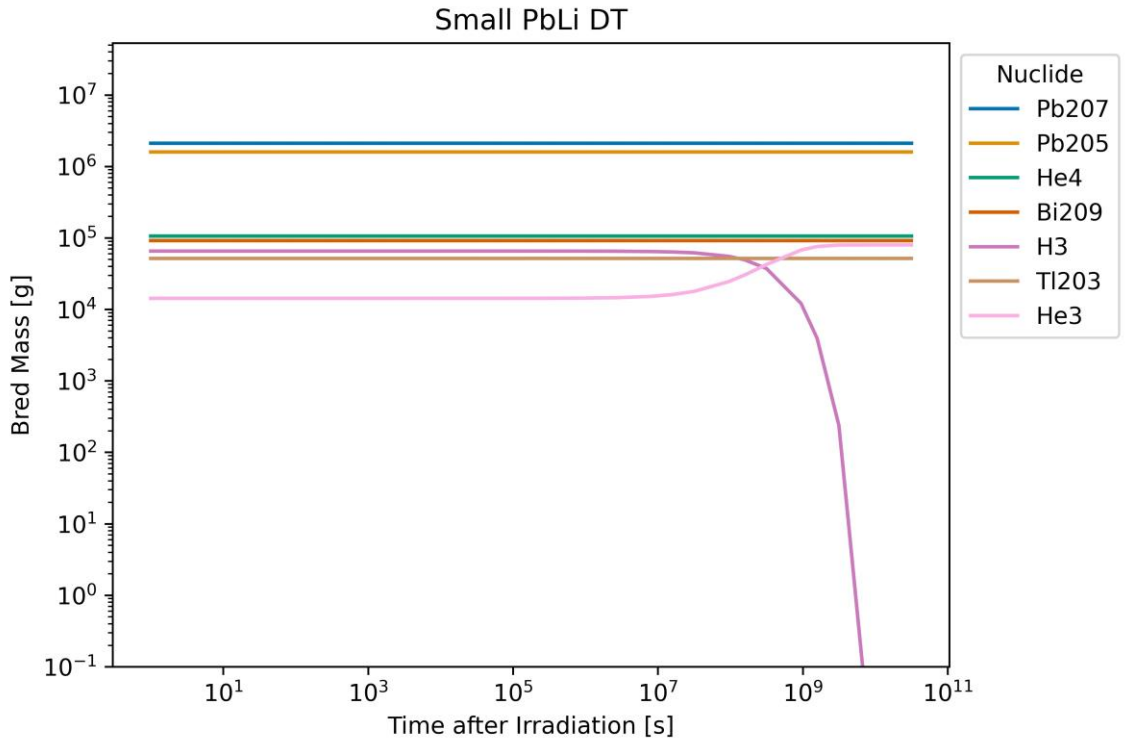

Figure 39: The dominant bred mass nuclides for a batch of liquid metal for the small, D-T, lithium-lead model.

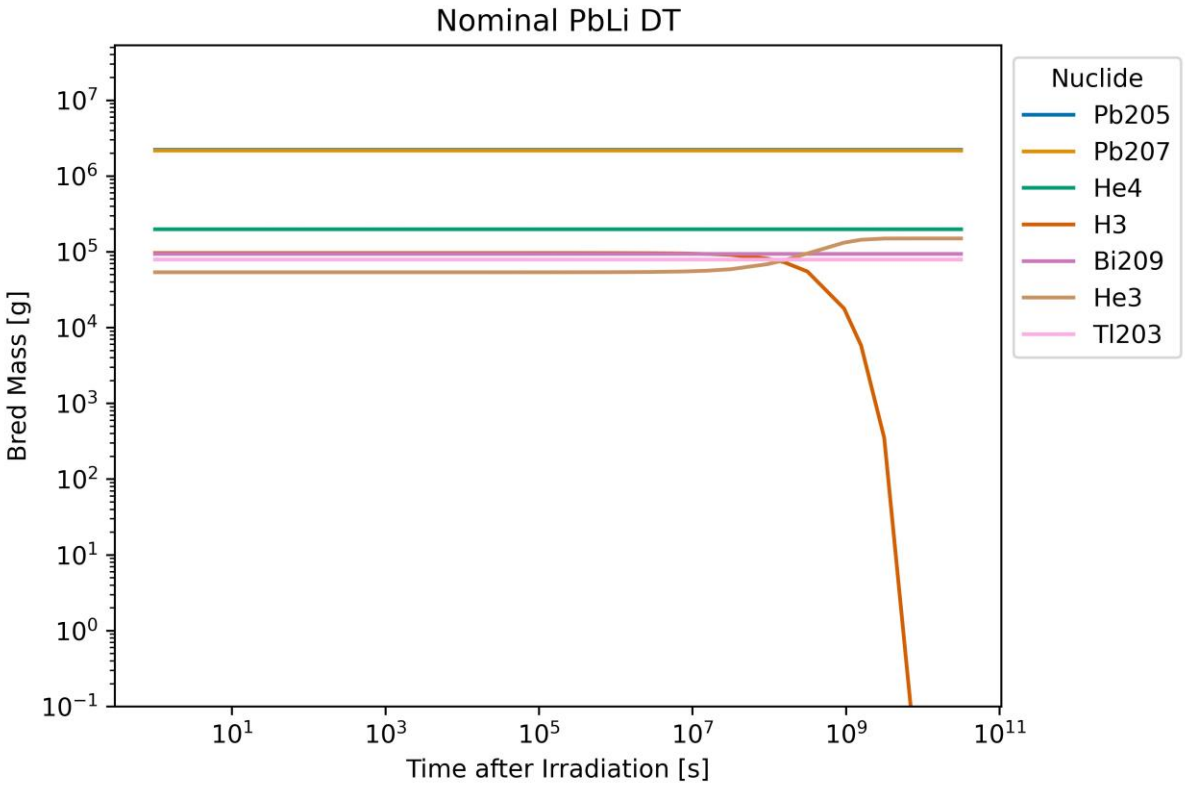

Figure 40: The dominant bred mass nuclides for a batch of liquid metal for the nominal, D-T, lithium-lead model.

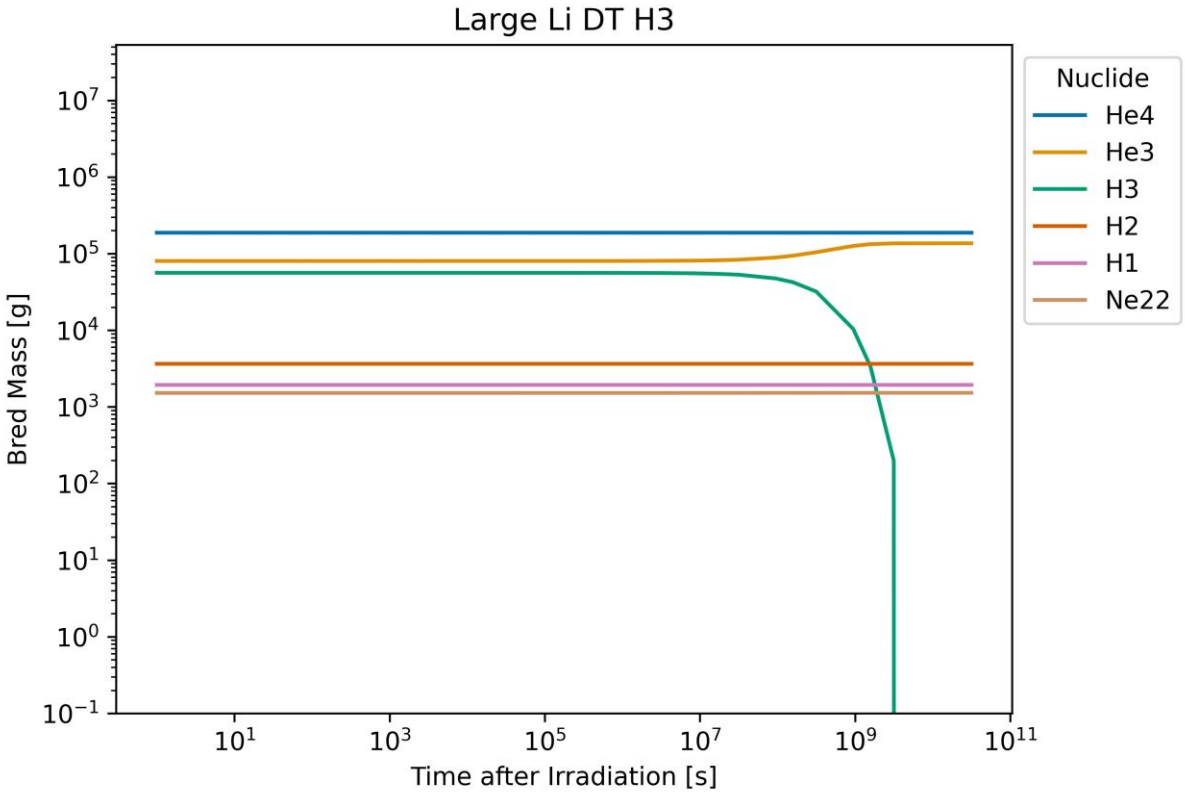

Figure 41: The dominant bred mass nuclides for a batch of liquid metal for the large, D-T, lithium model with trace tritium in the initial inventory.

7.9 Nuclide Inventory of the Liquid Metal (masses) (tables)

Table 13: The bred nuclide inventory for the small, D-T, lithium model, 1 day after end of irradiation.

Nuclide	Mass [g]		Nuclide	Mass [g]		Nuclide	Mass [g]
He4	1.68E+05		C13	4.50E-02		Mn56	1.14E-07
He3	6.26E+04		Mg25	2.81E-02		Sc44m	7.87E-08
H3	5.81E+04		C14	2.26E-02		Sc48	1.55E-08
H1	7.45E+03		Co59	1.60E-02		Sc44	5.78E-09
H2	4.17E+03		S35	1.24E-02		Ni62	4.48E-09
Ne22	1.67E+03		P31	7.28E-03		Ar41	1.15E-09
Ne20	6.85E+02		Ti49	6.74E-03		Co57	1.04E-09
K40	1.68E+02		Si30	4.20E-03		Co58m	9.34E-10
Ar38	1.62E+02		Ti46	4.05E-03		B10	5.18E-10
Mg24	1.33E+02		Ca45	3.35E-03		Ni58	2.78E-10
Ar39	1.12E+02		V50	3.11E-03		Al26	8.44E-11
Cl36	6.61E+01		Na24	2.68E-03		Si31	4.87E-11
Cl37	6.58E+01		Ti48	2.54E-03		V48	1.56E-11
Mn55	1.76E+01		Ti50	1.74E-03		F18	9.49E-12
Ne21	1.43E+01		C12	1.64E-03		Ni63	6.97E-12
F19	1.22E+01		P33	1.13E-03		Cu63	3.43E-13
Cl35	1.11E+01		Cr51	7.73E-04		Ti45	4.65E-14
Ca41	6.98E+00		Si29	5.53E-04		Ni64	4.41E-14
Ar36	5.60E+00		Cr50	3.28E-04		Co56	3.19E-14
Na22	5.08E+00		Ca47	1.54E-04		Cl39	1.24E-14
O17	4.36E+00		P32	1.38E-04		Ti44	6.34E-15
Ar40	3.89E+00		Sc47	1.32E-04		Sc45m	1.31E-15
Cr54	2.43E+00		Si28	1.16E-04		Sc49	9.38E-16
Cr53	2.42E+00		N14	1.05E-04		Mg28	6.42E-16
O16	2.24E+00		Fe59	7.23E-05		Co61	4.55E-16
Fe57	2.16E+00		Ni60	6.65E-05		Zn64	3.64E-16
Ca42	2.16E+00		Si32	5.47E-05		S38	3.33E-16
Ca43	1.71E+00		K42	4.20E-05		Cl38	1.33E-16
Fe55	1.70E+00		Co60	2.99E-05		Sc43	1.16E-16
Mn53	1.46E+00		Sc46	2.08E-05		Cu65	1.96E-17
S36	1.41E+00		Be10	1.90E-05		Co60m	1.17E-17
S34	5.88E-01		Mg26	6.97E-06		Ni57	1.10E-17
Ti47	4.00E-01		B11	6.15E-06		Fe52	4.39E-18
S33	3.59E-01		Al27	3.04E-06		Al28	1.15E-18
V51	2.92E-01		Mn52	1.95E-06		Mn52m	1.96E-19
Fe58	2.65E-01		K43	1.95E-06		Zn65	9.97E-20
Ar37	2.07E-01		Co58	1.85E-06		Cu64	8.55E-20
Sc45	2.03E-01		V49	1.79E-06		Zn66	2.02E-20
O18	1.85E-01		Ar42	1.14E-06		Cr48	5.83E-21
N15	9.67E-02		Be9	1.08E-06		Co55	1.73E-21
Mn54	8.05E-02		Fe60	8.79E-07		Cl34m	6.27E-22
Cr52	7.57E-02		Ni61	8.24E-07			
S32	5.65E-02		Ni59	1.50E-07			

Table 14: The bred nuclide inventory for the nominal, D-T, lithium model, 1 day after end of irradiation.

Nuclide	Mass [g]		Nuclide	Mass [g]		Nuclide	Mass [g]
He4	2.02E+05		S32	1.66E-02		Sc44m	2.59E-08
He3	8.33E+04		C13	1.12E-02		Ni59	1.98E-08
H3	6.28E+04		Mg25	1.09E-02		Sc48	4.62E-09
H2	4.09E+03		Ti49	8.62E-03		Sc44	1.90E-09
H1	3.78E+03		S35	4.91E-03		Ar41	1.17E-09
Ne22	1.69E+03		Ca45	3.69E-03		Co58m	3.24E-10
Ne20	6.96E+02		Na24	3.28E-03		Ni62	2.43E-10
K40	1.78E+02		C14	2.26E-03		Co57	1.07E-10
Ar38	1.64E+02		P31	1.90E-03		B10	1.76E-11
Mg24	1.64E+02		Ti46	1.31E-03		Ni58	1.09E-11
Ar39	1.15E+02		V50	9.56E-04		Si31	4.39E-12
Cl36	6.83E+01		Ti48	8.98E-04		F18	2.69E-12
Cl37	6.55E+01		Cr51	7.98E-04		Al26	1.54E-12
Mn55	1.79E+01		Si30	6.74E-04		V48	4.98E-13
F19	1.16E+01		Ti50	5.23E-04		Ni63	1.36E-13
Cl35	1.07E+01		P33	3.44E-04		Cu63	6.75E-15
Ne21	8.49E+00		Cr50	3.32E-04		Ti45	4.45E-15
Ca41	8.12E+00		Ca47	1.57E-04		Cl39	3.32E-15
Ar36	5.83E+00		C12	1.46E-04		Sc45m	1.45E-15
Na22	5.21E+00		Sc47	1.34E-04		Sc49	1.09E-15
Ar40	3.10E+00		Fe59	8.23E-05		Co56	9.78E-16
Fe57	2.73E+00		Si29	7.94E-05		Ni64	3.24E-16
Ca42	2.61E+00		K42	4.86E-05		Ti44	1.82E-16
Cr53	2.44E+00		P32	3.98E-05		S38	7.44E-17
Cr54	2.36E+00		Ni60	2.93E-05		Co61	6.97E-17
Fe55	1.73E+00		Co60	1.31E-05		Cl38	3.33E-17
Ca43	1.72E+00		Si32	1.21E-05		Mg28	1.82E-17
Mn53	1.53E+00		Si28	1.00E-05		Sc43	1.13E-17
O17	1.32E+00		N14	9.55E-06		Co60m	4.51E-18
O16	6.70E-01		Sc46	7.65E-06		Zn64	2.59E-18
S36	4.59E-01		K43	1.79E-06		Fe52	1.34E-18
Ti47	4.08E-01		Be10	1.46E-06		Ni57	1.28E-19
Fe58	3.24E-01		Mg26	8.15E-07		Mn52m	5.99E-20
V51	2.99E-01		Co58	6.44E-07		Cu65	5.01E-20
Sc45	2.26E-01		Mn52	6.06E-07		Al28	3.26E-20
Ar37	2.14E-01		B11	4.84E-07		K44	9.42E-22
S33	1.78E-01		Ar42	3.91E-07		Cu64	6.01E-22
S34	1.76E-01		Fe60	3.40E-07		Cr48	5.18E-22
Mn54	7.50E-02		V49	1.93E-07		Zn65	2.44E-22
O18	5.17E-02		Al27	1.73E-07			
Cr52	3.44E-02		Ni61	1.27E-07			
N15	2.80E-02		Mn56	1.13E-07			
Co59	1.86E-02		Be9	2.84E-08			

Table 15: The bred nuclide inventory for the large, D-T, lithium model, 1 day after end of irradiation.

Nuclide	Mass [g]		Nuclide	Mass [g]		Nuclide	Mass [g]
He4	2.09E+05		Ti49	8.95E-03		Ni59	3.72E-09
He3	8.89E+04		S32	7.08E-03		Be9	2.14E-09
H3	6.22E+04		Mg25	4.75E-03		Sc48	1.95E-09
H2	4.06E+03		C13	4.51E-03		Ar41	1.17E-09
H1	2.16E+03		Ca45	3.73E-03		Sc44	8.12E-10
Ne22	1.69E+03		Na24	3.36E-03		Co58m	1.39E-10
Ne20	6.98E+02		S35	3.08E-03		Ni62	2.00E-11
K40	1.80E+02		Cr51	8.04E-04		Co57	1.95E-11
Mg24	1.68E+02		P31	7.73E-04		B10	1.94E-12
Ar38	1.64E+02		Ti46	5.58E-04		F18	1.13E-12
Ar39	1.15E+02		C14	4.65E-04		Ni58	8.67E-13
Cl36	6.89E+01		V50	4.07E-04		Si31	8.04E-13
Cl37	6.52E+01		Ti48	3.87E-04		Al26	1.02E-13
Mn55	1.80E+01		Cr50	3.33E-04		V48	4.92E-14
F19	1.15E+01		Ti50	2.21E-04		Ni63	4.84E-15
Cl35	1.06E+01		Si30	2.20E-04		Cl39	1.51E-15
Ca41	8.31E+00		Ca47	1.58E-04		Sc45m	1.46E-15
Ne21	7.04E+00		P33	1.46E-04		Sc49	1.20E-15
Ar36	5.89E+00		Sc47	1.34E-04		Ti45	8.01E-16
Na22	5.24E+00		Fe59	8.30E-05		Cu63	2.40E-16
Ar40	2.87E+00		K42	4.95E-05		Co56	7.49E-17
Fe57	2.81E+00		C12	2.60E-05		Cl38	3.25E-17
Ca42	2.66E+00		Si29	2.47E-05		S38	2.88E-17
Cr53	2.45E+00		P32	1.68E-05		Ti44	1.38E-17
Cr54	2.33E+00		Ni60	1.30E-05		Co61	1.33E-17
Fe55	1.74E+00		Co60	5.83E-06		Ni64	5.01E-18
Ca43	1.72E+00		Si32	4.66E-06		Sc43	2.04E-18
Mn53	1.55E+00		Sc46	3.30E-06		Co60m	1.95E-18
O17	5.58E-01		N14	1.80E-06		Mg28	1.56E-18
Ti47	4.10E-01		Si28	1.80E-06		Fe52	5.71E-19
Fe58	3.29E-01		K43	1.75E-06		Zn64	3.99E-20
V51	3.01E-01		Co58	2.76E-07		Mn52m	2.55E-20
O16	2.83E-01		Mn52	2.59E-07		Ni57	4.28E-21
Sc45	2.28E-01		Be10	2.50E-07		Al28	2.79E-21
Ar37	2.16E-01		Ar42	1.74E-07		Cu65	3.33E-22
S36	1.96E-01		Mg26	1.49E-07		Cr48	9.25E-23
S33	1.32E-01		Fe60	1.47E-07		Cl34m	8.77E-23
S34	7.44E-02		Mn56	1.12E-07			
Mn54	7.34E-02		B11	8.36E-08			
Cr52	2.41E-02		V49	4.50E-08			
O18	2.14E-02		Al27	2.62E-08			
Co59	1.90E-02		Ni61	2.43E-08			
N15	1.18E-02		Sc44m	1.11E-08			

Table 16: The bred nuclide inventory for the small, D-T, lithium-lead model, 1 day after end of irradiation

Nuclide	Mass [g]		Nuclide	Mass [g]		Nuclide	Mass [g]		Nuclide	Mass [g]
Pb207	2.34E+06		S36	2.94E-01		Bi206	9.64E-05		Be9	3.11E-09
Pb205	1.77E+06		Po209	2.18E-01		Ni62	6.14E-05		Sc44	2.91E-09
He4	1.18E+05		Sc45	2.07E-01		K42	5.80E-05		Sc48	1.01E-09
Bi209	1.02E+05		Fe55	1.83E-01		V50	4.58E-05		Co58m	9.55E-10
H3	7.26E+04		Cr54	1.70E-01		Cr51	4.19E-05		Zn64	7.81E-10
Tl203	5.73E+04		Pb202	1.61E-01		Cr50	3.04E-05		Tl206	5.66E-10
H1	3.21E+04		Cr53	1.30E-01		Hg198	2.78E-05		Cu65	4.36E-10
He3	1.58E+04		O17	6.36E-02		Fe60	2.30E-05		Co57	3.72E-10
Tl205	7.34E+03		Pb210	5.94E-02		P33	2.06E-05		Au198	2.07E-10
Tl204	6.45E+03		O16	5.07E-02		C12	1.81E-05		Hg196	1.69E-10
Hg204	3.10E+03		Mn53	4.51E-02		Pt198	1.77E-05		Hg197	1.43E-10
Bi208	9.93E+02		Ti49	3.86E-02		Ca47	1.13E-05		Pt195	6.13E-11
Hg202	7.42E+02		Co59	3.75E-02		Si29	1.04E-05		Ar41	5.52E-11
H2	3.14E+02		Ti47	2.81E-02		Sc47	9.65E-06		Pt197	4.75E-11
Mg24	2.64E+02		S34	2.06E-02		Tl201	8.97E-06		Hg197m	1.82E-11
Ne22	1.11E+02		Ca43	1.87E-02		Ni59	6.50E-06		Po207	1.54E-11
Ne20	3.57E+01		V51	1.55E-02		P32	2.73E-06		Tl200	1.46E-11
K40	3.07E+01		S33	1.39E-02		N14	2.64E-06		Pt200	9.85E-12
Bi210m	2.16E+01		Ti46	1.07E-02		Si32	2.04E-06		Au196	5.57E-12
Po210	2.12E+01		Ar37	1.01E-02		Co58	1.87E-06		Zn66	5.18E-12
Hg201	1.78E+01		Ni60	8.29E-03		Si28	1.13E-06		Al26	2.83E-12
Pb203	1.35E+01		Pb209	7.80E-03		Ni63	1.07E-06		B10	2.11E-12
Ar38	1.06E+01		O18	6.77E-03		Au200m	9.76E-07		Zn65	1.94E-12
Ar39	7.59E+00		Mn54	6.06E-03		Ar42	5.08E-07		Pt194	7.41E-13
Bi207	6.81E+00		Na24	5.27E-03		Au197	4.26E-07		Co61	6.56E-13
Fe57	5.79E+00		Hg199	4.12E-03		Au199	3.07E-07		Si31	6.08E-13
Ca41	5.59E+00		Co60	3.75E-03		Al27	1.94E-07		F18	4.15E-13
Cl37	5.05E+00		Ca45	3.57E-03		Be10	1.21E-07		Au198m	4.07E-13
Ca42	4.98E+00		Cr52	3.35E-03		B11	1.20E-07		Cu64	1.82E-13
Cl36	2.58E+00		N15	2.73E-03		Ni64	1.16E-07		Ti45	8.11E-14
Hg203	2.26E+00		Ti48	1.89E-03		K43	1.04E-07		Pb200	7.78E-14
Mn55	1.61E+00		S32	1.27E-03		Cu63	5.22E-08		V48	6.79E-14
Ar40	1.55E+00		C14	1.26E-03		Sc44m	3.97E-08		Au195	6.55E-14
Tl202	1.39E+00		Ni61	1.12E-03		Mn52	3.24E-08		Pt195m	6.42E-14
F19	1.14E+00		C13	1.04E-03		Pb204m	2.34E-08		Zn67	3.39E-14
Ne21	9.71E-01		Si30	6.28E-04		Pb201	1.69E-08		Pt202	2.31E-14
Cl35	7.93E-01		Ti50	5.98E-04		V49	1.52E-08		Ir193	1.04E-14
Fe58	7.61E-01		Po208	4.75E-04		Mn56	1.45E-08		Pb212	1.03E-14
Bi210	6.76E-01		S35	4.52E-04		Pb202m	1.32E-08		Po206	5.43E-15
Hg200	6.16E-01		Mg26	4.20E-04		Pt196	1.06E-08		Co56	5.33E-15
Ar36	4.54E-01		Fe59	2.95E-04		Au200	7.93E-09		Ti44	4.33E-15
Na22	4.15E-01		P31	2.31E-04		Ni58	4.98E-09		Sc49	3.82E-15
Mg25	3.04E-01		Sc46	1.77E-04		Bi205	3.85E-09		Au196n	3.56E-15

Table 16 (cont):

Zn68	3.25E-15		Mn52m	1.00E-20
Pt193	2.64E-15		Cu66	9.06E-21
Os194	1.45E-15		Zn70	8.10E-21
Sc45m	1.40E-15		Cu67	6.52E-21
Bi212	1.08E-15		Al28	5.77E-21
Bi204	8.42E-16		Ge72	1.25E-21
Hg206	7.74E-16		Au195m	1.00E-21
Co60m	3.05E-16		Au201	9.31E-22
Hg195m	2.95E-16		Zn69m	8.75E-22
Cl39	1.86E-16		Bi203	6.61E-22
Os192	1.65E-16		Ge71	3.23E-22
Au197m	1.41E-16		Cr48	1.59E-22
Ni57	1.11E-16		K44	1.47E-22
Pt197m	8.79E-17		Co55	1.16E-22
Hg195	5.57E-17			
Pt192	5.42E-17			
Ir194	4.70E-17			
Ga69	4.31E-17			
Ni65	3.64E-17			
Sc43	2.48E-17			
Tl208	1.92E-17			
Ni66	5.79E-18			
Ir193m	5.78E-18			
S38	5.23E-18			
Au202	4.20E-18			
Os193	4.19E-18			
Pt193m	4.19E-18			
Mg28	3.22E-18			
Ir191	2.44E-18			
Pb205m	2.08E-18			
Tl199	1.88E-18			
Ge70	1.84E-18			
Ir192	1.73E-18			
Hg194	1.60E-18			
Ir192n	1.05E-18			
Cl38	8.67E-19			
Au196m	8.14E-19			
Fe52	2.25E-19			
Au194	1.35E-19			
Ir195	8.76E-20			
Hg199m	5.80E-20			
Os190	3.19E-20			
Os191	2.97E-20			
Ga71	2.39E-20			

Table 17: The bred nuclide inventory for the nominal, D-T, lithium-lead model, 1 day after end of irradiation.

Nuclide	Mass [g]	Nuclide	Mass [g]	Nuclide	Mass [g]	Nuclide	Mass [g]
Pb205	2.46E+06	Fe55	1.92E-01	Cr50	3.20E-05	Tl206	2.06E-10
Pb207	2.42E+06	Cr54	1.37E-01	V50	2.03E-05	Ni58	1.95E-10
He4	2.22E+05	Cr53	1.36E-01	Po208	1.34E-05	Be9	8.12E-11
H3	1.07E+05	Pb202	1.00E-01	Ca47	1.16E-05	Ar41	5.22E-11
Bi209	1.04E+05	S36	9.69E-02	Sc47	9.83E-06	Bi205	3.82E-11
Tl203	8.74E+04	Mg25	9.56E-02	Pt198	7.05E-06	Co57	3.48E-11
He3	5.95E+04	Mn53	7.95E-02	P33	6.79E-06	Au198	1.39E-11
H1	2.89E+04	Ti49	4.28E-02	Fe60	5.79E-06	Hg196	1.30E-11
Tl204	3.50E+03	Co59	3.81E-02	Bi206	3.22E-06	Pt197	8.54E-12
Hg204	2.80E+03	Ti47	2.96E-02	Hg198	2.70E-06	Hg197	4.12E-12
Tl205	1.28E+03	Po209	2.07E-02	Si29	2.29E-06	Pt195	2.99E-12
Bi208	3.70E+02	Pb210	1.94E-02	Ni62	2.19E-06	Zn64	2.86E-12
Hg202	3.07E+02	O17	1.92E-02	C12	1.59E-06	Pt200	2.28E-12
H2	2.89E+02	V51	1.62E-02	Tl201	1.24E-06	Tl200	6.11E-13
Mg24	2.78E+02	O16	1.51E-02	Ni59	8.92E-07	Hg197m	5.26E-13
Ne22	1.12E+02	S33	1.07E-02	P32	8.58E-07	Cu65	4.76E-13
Ne20	3.59E+01	Ar37	1.01E-02	Co58	5.72E-07	Au196	3.44E-13
K40	3.51E+01	Pb209	7.89E-03	Au200m	4.42E-07	Po207	1.29E-13
Hg201	2.13E+01	S34	6.00E-03	Si32	3.80E-07	F18	1.21E-13
Bi210m	1.88E+01	Na24	5.55E-03	N14	2.48E-07	B10	1.12E-13
Pb203	1.56E+01	Mn54	4.92E-03	Ar42	1.57E-07	Al26	7.37E-14
Ar38	9.89E+00	Ca45	3.66E-03	Au199	1.14E-07	Co61	7.10E-14
Ar39	8.13E+00	Ti46	3.47E-03	Si28	1.04E-07	Si31	5.45E-14
Ca41	7.34E+00	Ni60	3.02E-03	K43	1.00E-07	Au198m	4.76E-14
Po210	6.49E+00	Cr52	2.11E-03	Au197	8.87E-08	Pt194	3.27E-14
Fe57	6.33E+00	O18	1.94E-03	Mn52	1.69E-08	Ti45	7.76E-15
Ca42	4.75E+00	Co60	1.34E-03	Pb204m	1.65E-08	Sc49	4.30E-15
Cl37	3.73E+00	Hg199	1.23E-03	Al27	1.33E-08	Pb200	4.26E-15
Cl36	2.95E+00	N15	8.22E-04	Sc44m	1.25E-08	V48	4.16E-15
Mn55	1.85E+00	Ti48	6.06E-04	Ni63	1.25E-08	Zn65	2.22E-15
Hg203	1.65E+00	S32	3.99E-04	Be10	1.02E-08	Pt195m	2.10E-15
F19	1.12E+00	C13	2.97E-04	B11	9.16E-09	Pt202	2.04E-15
Cl35	8.04E-01	S35	2.37E-04	Mn56	8.91E-09	Zn66	1.75E-15
Bi207	7.68E-01	Fe59	2.03E-04	Pb202m	4.48E-09	Au195	1.54E-15
Ne21	6.46E-01	Ti50	2.00E-04	Au200	3.59E-09	Sc45m	1.43E-15
Ar40	6.33E-01	Si30	1.54E-04	Pb201	3.12E-09	Cu64	6.70E-16
Tl202	6.30E-01	Ni61	1.30E-04	V49	3.12E-09	Ir193	5.12E-16
Fe58	6.15E-01	C14	1.20E-04	Pt196	1.07E-09	Pb212	3.49E-16
Ar36	4.85E-01	P31	6.63E-05	Sc44	9.21E-10	Hg206	2.53E-16
Na22	4.72E-01	K42	6.06E-05	Cu63	6.17E-10	Au196n	2.19E-16
Hg200	4.13E-01	Sc46	5.78E-05	Ni64	4.17E-10	Os194	1.88E-16
Sc45	2.21E-01	Cr51	4.34E-05	Co58m	2.87E-10	Co56	1.55E-16
Bi210	2.08E-01	Mg26	3.97E-05	Sc48	2.81E-10	Ti44	1.27E-16

Table 17 (cont):

Co60m	7.68E-17
Cl39	6.15E-17
Pt193	4.94E-17
Bi212	3.65E-17
Pt197m	1.48E-17
Po206	1.35E-17
Hg195m	6.77E-18
Au197m	4.07E-18
Zn67	3.71E-18
Os192	3.63E-18
Ir194	2.88E-18
Bi204	2.47E-18
Sc43	2.31E-18
Ni57	1.28E-18
Hg195	1.28E-18
S38	1.11E-18
Pt192	9.24E-19
Cl38	6.56E-19
Tl208	6.53E-19
Au202	3.70E-19
Ir193m	3.28E-19
Hg199m	1.73E-19
Os193	1.26E-19
Zn68	1.12E-19
Mg28	1.06E-19
Fe52	6.91E-20
Pt193m	5.84E-20
Au196m	5.02E-20
Ir191	4.61E-20
Ni65	3.96E-20
Ir192n	3.78E-20
Ir192	2.49E-20
Tl199	2.47E-20
Pb205m	2.06E-20
Hg194	1.27E-20
Ir195	1.02E-20
Mn52m	3.08E-21
Ni66	1.99E-21
Pb211	1.58E-21
Au194	9.38E-22
Ga69	4.81E-22
Os191	3.73E-22
Os190	3.62E-22
Al28	1.89E-22

Table 18: The bred nuclide inventory for the large, D-T, lithium-lead model, 1 day after end of irradiation.

Nuclide	Mass [g]	Nuclide	Mass [g]	Nuclide	Mass [g]	Nuclide	Mass [g]
Pb205	2.69E+06	Cr53	1.38E-01	Ca47	1.16E-05	Cu63	2.06E-11
Pb207	2.43E+06	Cr54	1.22E-01	Sc47	9.88E-06	Ni58	1.59E-11
He4	2.66E+05	Mn53	9.51E-02	V50	9.69E-06	Co57	6.34E-12
H3	1.06E+05	Bi210	8.37E-02	Mg26	7.10E-06	Be9	6.11E-12
Bi209	1.04E+05	Pb202	5.32E-02	Pt198	3.32E-06	Ni64	5.86E-12
Tl203	9.85E+04	Ti49	4.31E-02	P33	2.95E-06	Pt197	2.80E-12
He3	9.42E+04	S36	4.18E-02	Fe60	2.30E-06	Au198	2.23E-12
H1	1.75E+04	Mg25	4.05E-02	Po208	9.76E-07	Hg196	2.21E-12
Hg204	2.63E+03	Co59	3.84E-02	Si29	8.80E-07	Bi205	1.30E-12
Tl204	1.73E+03	Ti47	3.00E-02	Hg198	4.87E-07	Pt200	9.05E-13
Tl205	3.79E+02	V51	1.64E-02	P32	3.78E-07	Pt195	3.74E-13
Mg24	2.78E+02	Ar37	1.00E-02	C12	2.84E-07	Hg197	3.13E-13
H2	2.78E+02	S33	9.79E-03	Bi206	2.59E-07	Tl200	5.50E-14
Bi208	1.66E+02	Pb210	8.26E-03	Tl201	2.51E-07	Au196	5.42E-14
Hg202	1.46E+02	O17	8.12E-03	Co58	2.45E-07	F18	5.29E-14
Ne22	1.12E+02	Pb209	7.95E-03	Au200m	2.10E-07	Zn64	4.05E-14
K40	3.61E+01	O16	6.36E-03	Ni59	1.75E-07	Hg197m	4.00E-14
Ne20	3.59E+01	Na24	5.56E-03	Ni62	1.71E-07	B10	1.40E-14
Hg201	2.37E+01	Mn54	4.14E-03	Si32	1.35E-07	Co61	1.38E-14
Pb203	1.61E+01	Ca45	3.66E-03	K43	9.93E-08	Si31	1.08E-14
Bi210m	1.32E+01	Po209	3.57E-03	Ar42	6.74E-08	Au198m	9.66E-15
Ar38	9.63E+00	S34	2.51E-03	Au199	5.14E-08	Sc49	6.48E-15
Ar39	8.29E+00	Cr52	1.76E-03	N14	4.74E-08	Al26	5.50E-15
Ca41	7.85E+00	Ti46	1.48E-03	Au197	3.31E-08	Pt194	4.70E-15
Fe57	6.41E+00	Ni60	1.31E-03	Si28	1.99E-08	Po207	3.95E-15
Ca42	4.62E+00	O18	8.10E-04	Pb204m	1.75E-08	Cu65	2.83E-15
Cl37	3.35E+00	Co60	5.84E-04	Mn52	8.54E-09	Sc45m	1.44E-15
Cl36	3.06E+00	Hg199	5.08E-04	Mn56	7.24E-09	Ti45	1.40E-15
Po210	2.62E+00	N15	3.48E-04	Sc44m	5.35E-09	V48	6.04E-16
Mn55	1.91E+00	Ti48	2.59E-04	Al27	2.17E-09	Pb200	4.02E-16
Hg203	1.56E+00	S35	1.87E-04	Pb202m	1.97E-09	Pt202	3.85E-16
F19	1.11E+00	Fe59	1.82E-04	Be10	1.79E-09	Pt195m	2.11E-16
Cl35	8.08E-01	S32	1.78E-04	Au200	1.71E-09	Au195	1.11E-16
Fe58	5.70E-01	C13	1.24E-04	B11	1.57E-09	Hg206	1.08E-16
Ne21	5.64E-01	Ti50	8.50E-05	V49	1.07E-09	Ir193	6.46E-17
Ar36	4.93E-01	K42	6.11E-05	Pb201	6.99E-10	Cl39	4.12E-17
Na22	4.90E-01	Si30	6.09E-05	Ni63	4.16E-10	Os194	3.81E-17
Ar40	3.67E-01	Cr51	4.38E-05	Sc44	3.93E-10	Au196n	3.45E-17
Hg200	3.41E-01	Cr50	3.24E-05	Pt196	2.37E-10	Co60m	3.05E-17
Tl202	2.99E-01	P31	2.78E-05	Co58m	1.22E-10	Pb212	2.66E-17
Sc45	2.23E-01	Sc46	2.47E-05	Sc48	1.16E-10	Zn65	1.33E-17
Fe55	1.94E-01	Ni61	2.40E-05	Tl206	9.76E-11	Co56	1.20E-17
Bi207	1.46E-01	C14	2.34E-05	Ar41	5.43E-11	Ti44	9.71E-18

Table 18 (cont):

Cu64	9.46E-18
Pt197m	4.98E-18
Zn66	4.44E-18
Pt193	3.40E-18
Bi212	2.79E-18
Cl38	1.60E-18
Hg195m	4.86E-19
Ir194	4.55E-19
S38	4.37E-19
Sc43	4.18E-19
Au197m	3.10E-19
Os192	2.91E-19
Hg199m	1.75E-19
Po206	1.75E-19
Hg195	9.16E-20
Au202	7.00E-20
Pt192	5.51E-20
Ir193m	5.05E-20
Tl208	4.98E-20
Ni57	4.43E-20
Bi204	3.54E-20
Fe52	2.94E-20
Os193	1.17E-20
Mg28	1.13E-20
Au196m	7.90E-21
Zn67	4.11E-21
Pt193m	3.62E-21
Ir192n	3.25E-21
Ir191	2.93E-21
Ir195	2.06E-21
Pb211	1.53E-21
Mn52m	1.31E-21
Ir192	1.30E-21
Tl199	1.03E-21
Pb205m	6.99E-22
Hg194	4.04E-22
Ni65	2.38E-22

Table 19: The bred nuclide inventory for the large, D-T, lithium model with Supplier 2 impurities, 1 day after end of irradiation.

Nuclide	Mass [g]	Nuclide	Mass [g]	Nuclide	Mass [g]	Nuclide	Mass [g]
He4	2.08E+05	Co59	7.44E-01	Fe60	1.38E-04	Ni66	3.58E-12
He3	8.86E+04	Tl203	4.57E-01	Fe59	1.21E-04	Bi206	3.35E-12
H3	6.21E+04	Ar40	3.41E-01	Ti50	1.09E-04	Au200m	1.95E-12
H2	4.03E+03	Co60	3.16E-01	Hg201	9.00E-05	Ni56	9.89E-13
H1	2.06E+03	F19	2.53E-01	Ca47	7.82E-05	Ge70	5.53E-13
K40	7.69E+01	Ti47	2.03E-01	Pb203	7.06E-05	Au199	4.34E-13
Ne22	3.83E+01	Co57	1.76E-01	Sc47	6.65E-05	Au197	3.35E-13
Cl37	2.67E+01	V51	1.49E-01	Si32	3.38E-05	Po208	3.15E-13
B11	2.51E+01	S33	1.31E-01	Co58m	2.32E-05	Mg28	1.83E-13
C14	2.08E+01	Al26	1.19E-01	Ni57	1.50E-05	Pb204m	1.16E-13
Ne20	1.89E+01	Na22	1.15E-01	K42	7.43E-06	F18	2.47E-14
Ar38	1.66E+01	Sc45	1.13E-01	Hg203	5.29E-06	Pb201	2.43E-14
S34	1.64E+01	Ar37	1.07E-01	Tl202	3.89E-06	V48	2.40E-14
K39	1.55E+01	S35	9.65E-02	Zn68	2.23E-06	Pb202m	2.10E-14
Ni62	1.29E+01	Co58	6.79E-02	Sc46	1.65E-06	Au200	1.58E-14
Ar39	1.28E+01	Bi209	5.26E-02	Hg200	1.51E-06	Cu66	5.60E-15
Cl36	1.25E+01	Mn54	3.65E-02	Bi210m	1.10E-06	Co55	5.45E-15
Pb207	1.19E+01	O17	1.73E-02	K43	8.69E-07	Zn69m	4.98E-15
Mn55	1.03E+01	Cr52	1.20E-02	Co56	7.97E-07	Pt196	3.69E-15
Ni64	1.03E+01	Ca42	1.20E-02	Pb202	7.33E-07	Zn70	2.33E-15
Mg25	1.00E+01	Hg204	8.40E-03	Bi207	6.65E-07	Co60m	1.83E-15
Fe58	9.91E+00	P32	7.78E-03	Mn52	1.27E-07	Sc45m	7.23E-16
Ne21	9.23E+00	O16	7.67E-03	Po210	1.00E-07	Cu61	5.85E-16
Pb205	8.93E+00	Ti49	4.31E-03	Ar42	6.30E-08	Sc49	5.58E-16
Fe57	8.35E+00	O18	4.00E-03	Mn56	5.58E-08	Ti45	3.94E-16
Mg26	7.92E+00	Ca45	1.84E-03	V49	2.21E-08	Zn69	3.64E-16
Zn64	6.53E+00	Hg202	1.74E-03	Hg199	5.64E-09	Al28	3.28E-16
C13	6.28E+00	Be9	1.08E-03	Sc44m	5.44E-09	Ga71	2.37E-16
S32	5.77E+00	Zn67	9.78E-04	Pb209	4.00E-09	Cl39	1.60E-16
Ca41	4.12E+00	Be10	5.57E-04	Bi210	3.20E-09	Hg196	5.59E-17
C12	3.88E+00	Tl205	4.88E-04	Ni65	2.52E-09	Bi205	4.83E-17
Ni59	3.46E+00	B10	4.85E-04	Sc48	9.60E-10	Pt197	2.75E-17
Ar36	2.92E+00	Tl204	4.54E-04	Si31	7.61E-10	Hg197	2.59E-17
Ni63	2.42E+00	Cr51	3.99E-04	Ga69	5.89E-10	Pt195	1.32E-17
Zn66	2.10E+00	Zn65	3.79E-04	Sc44	3.99E-10	Ti44	6.76E-18
Cr53	1.21E+00	Na24	3.60E-04	Po209	3.94E-10	S38	6.64E-18
Cr54	1.16E+00	Ti46	2.76E-04	Pb210	2.76E-10	Zn62	6.26E-18
S36	1.09E+00	Bi208	2.53E-04	Ar41	1.53E-10	Au198	5.47E-18
Fe55	1.01E+00	Cu64	2.33E-04	Cu67	2.90E-11	Pt200	5.35E-18
P31	1.01E+00	V50	2.01E-04	Pt198	2.37E-11	Cl38	5.32E-18
Ca43	8.54E-01	Ti48	1.98E-04	Hg198	1.47E-11	Tl206	5.28E-18
Ni61	8.21E-01	P33	1.70E-04	Tl201	9.21E-12	Tl200	5.14E-18
Mn53	7.66E-01	Cr50	1.65E-04	Co61	6.81E-12	Hg197m	3.18E-18

Table 19 (cont):

Ge71	1.50E-18
Au196	1.49E-18
Sc43	9.98E-19
Fe52	2.81E-19
Au198m	1.84E-19
Ge72	1.59E-19
Cu62	1.12E-19
Pt194	1.07E-19
Ge69	6.74E-20
Zn63	4.30E-20
Pb200	3.64E-20
Cl34m	3.58E-20
Mn52m	1.25E-20
Pt195m	8.37E-21
Au195	7.55E-21
Po207	3.51E-21
Ir193	1.62E-21
K44	1.03E-21
Au196n	8.11E-22
Pt202	5.65E-22
Os194	4.54E-22

Table 20: The bred nuclide inventory for the large, D-T, lithium model with trace tritium, 1 day after end of irradiation.

Nuclide	Mass [g]		Nuclide	Mass [g]		Nuclide	Mass [g]
He4	2.09E+05		N15	1.17E-02		Ni61	2.43E-08
He3	8.91E+04		Ti49	8.94E-03		Sc44m	1.10E-08
H3	6.24E+04		S32	7.07E-03		Ni59	3.72E-09
H2	4.07E+03		Mg25	4.75E-03		Be9	2.14E-09
H1	2.17E+03		C13	4.51E-03		Sc48	1.95E-09
Ne22	1.69E+03		Ca45	3.72E-03		Ar41	1.17E-09
Ne20	6.98E+02		Na24	3.36E-03		Sc44	8.09E-10
K40	1.80E+02		S35	3.08E-03		Co58m	1.39E-10
Mg24	1.68E+02		Cr51	8.03E-04		Ni62	2.00E-11
Ar38	1.64E+02		P31	7.72E-04		Co57	1.95E-11
Ar39	1.15E+02		Ti46	5.57E-04		B10	1.94E-12
Cl36	6.88E+01		C14	4.64E-04		F18	1.12E-12
Cl37	6.52E+01		V50	4.07E-04		Ni58	8.66E-13
Mn55	1.80E+01		Ti48	3.87E-04		Si31	8.03E-13
F19	1.15E+01		Cr50	3.33E-04		Al26	1.02E-13
Cl35	1.06E+01		Ti50	2.21E-04		V48	4.92E-14
Ca41	8.31E+00		Si30	2.20E-04		Ni63	4.84E-15
Ne21	7.04E+00		Ca47	1.58E-04		Sc45m	1.46E-15
Ar36	5.89E+00		P33	1.46E-04		Cl39	1.41E-15
Na22	5.24E+00		Sc47	1.34E-04		Sc49	1.13E-15
Ar40	2.87E+00		Fe59	8.29E-05		Ti45	7.99E-16
Fe57	2.81E+00		K42	4.94E-05		Cu63	2.40E-16
Ca42	2.66E+00		C12	2.60E-05		Co56	7.48E-17
Cr53	2.45E+00		Si29	2.47E-05		S38	2.87E-17
Cr54	2.33E+00		P32	1.68E-05		Cl38	2.30E-17
Fe55	1.74E+00		Ni60	1.30E-05		Ti44	1.38E-17
Ca43	1.72E+00		Co60	5.83E-06		Co61	1.33E-17
Mn53	1.54E+00		Si32	4.65E-06		Ni64	5.01E-18
O17	5.58E-01		Sc46	3.29E-06		Sc43	2.03E-18
Ti47	4.10E-01		N14	1.80E-06		Co60m	1.95E-18
Fe58	3.29E-01		Si28	1.79E-06		Mg28	1.55E-18
V51	3.01E-01		K43	1.75E-06		Fe52	5.70E-19
O16	2.83E-01		Co58	2.76E-07		Zn64	3.99E-20
Sc45	2.28E-01		Mn52	2.58E-07		Mn52m	2.54E-20
Ar37	2.15E-01		Be10	2.50E-07		Ni57	4.28E-21
S36	1.96E-01		Ar42	1.74E-07		Al28	2.78E-21
S33	1.32E-01		Mg26	1.49E-07		Cu65	3.33E-22
S34	7.43E-02		Fe60	1.47E-07		Cr48	9.24E-23
Mn54	7.33E-02		Mn56	1.12E-07			
Cr52	2.41E-02		B11	8.36E-08			
O18	2.14E-02		V49	4.50E-08			
Co59	1.90E-02		Al27	2.62E-08			